

University of Alberta

**Identification and analysis of Tef1p, a novel Rho1p-
interacting protein**

by

James A. R. Bodman

A thesis submitted to the Faculty of Graduate Studies and Research
in partial fulfillment of the requirements for the degree of

Master of Science

Cell Biology

©James A. R. Bodman
Spring 2014
Edmonton, Alberta

Permission is hereby granted to the University of Alberta Libraries to reproduce single copies of this thesis and to lend or sell such copies for private, scholarly or scientific research purposes only. Where the thesis is converted to, or otherwise made available in digital form, the University of Alberta will advise potential users of the thesis of these terms.

The author reserves all other publication and other rights in association with the copyright in the thesis and, except as herein before provided, neither the thesis nor any substantial portion thereof may be printed or otherwise reproduced in any material form whatsoever without the author's prior written permission.

ABSTRACT

Rho GTPases act as molecular switches, occupying an active GTP or an inactive GDP-bound state. Rho1p, one member of the Rho family GTPases, has a role in the late stages of vacuole fusion through an unknown mechanism. We identified a ~50kDa Rho1p-interacting protein as Tef1p, a dual function GTPase with known roles in both protein translation and actin cytoskeletal organization. Tef1p is an aminoacyl-tRNA transferase in protein translation where GTP-bound Tef1p shuttles aminoacyl-charged tRNAs to ribosomes where they are transferred to the elongating peptide chain. Tef1p also binds actin filaments and organizes them into higher order cable structures such as stress fibers. We used nucleotide-state specific affinity pulldown methods to determine that Tef1p specifically interacts with Rho1p, but not as a downstream effector. The Tef1p::Rho1p interaction was calcium-dependent, suggesting that the interaction occurs late in membrane fusion. Our data suggest that Tef1p modulates Rho1p function, perhaps via complex formation.

ACKNOWLEDGEMENTS

I would like to start by thanking my supervisor Dr. Gary Eitzen for his guidance over the past 28 months. Thank you also to Dr. Paul LaPointe and Dr. Sarah Hughes for taking part in my committee. I would also like to thank past lab mates, Alicia Baier, Matt Baron, Azra Lari, and Vivian Nkafu. It has been great to work with all of you. I would also like to thank my friends and family for all of their support over the last two and some years.

TABLE OF CONTENTS

CHAPTER 1 INTRODUCTION	1
1.1 Membrane Fusion	2
1.2 Actin Dynamics	4
1.3 Rho GTPases	5
1.4 Translation Elongation Factor Tef1p	7
1.4.1 Canonical role in protein translation	7
1.4.2 Actin bundling properties	8
1.5 Focus and goals of this thesis	9
CHAPTER 2 MATERIALS AND METHODS	12
2.1 Oligonucleotides	13
2.2 Plasmids	14
2.3 Antibodies	14
2.4 Drugs	15
2.5 Microorganism strains and growth conditions	15
2.5.1 Bacterial strains	15
2.5.2 Yeast strains	16
2.6 Transformation of microorganisms	16
2.6.1 Bacterial Transformation	16
2.6.2 Lithium Acetate Yeast Transformation	17
2.7 Protein expression, lysate preparation, and protein purification	18

2.7.1 Bacterial protein expression and lysate preparation	18
2.7.2 Yeast protein expression and lysate preparation	18
2.7.3 Protein Purification	19
2.7.3.1 GST-fusion protein purification	19
2.7.3.2 MBP-fusion protein purification	20
2.8 Yeast vacuole membrane preparation	20
2.9 Biochemical assays	21
2.9.1 Affinity pulldown	21
2.9.1.1 Chemical nucleotide exchange	22
2.9.1.2 Quantification of binding	22
2.9.2 Co-immunoprecipitation	23
2.9.3 In vitro vacuole fusion assay	24
2.10 Microscopy	24
2.10.1 Yeast live whole-cell wide-field microscopy	24
2.10.2 Yeast fixed whole-cell wide-field microscopy	25
2.10.3 Yeast vacuole wide-field microscopy	26
2.10.4 Yeast growth curves	26
CHAPTER 3 RESULTS	27
3.1 Identification of a vacuolar Tef1p::Rho1p interaction	28
3.2 Tef1p is enriched on vacuole membranes	29
3.3 Nucleotide dependence of the Tef1p::Rho1p interaction	34
3.4 Analysis of Tef1p sub-domains for Rho1p interaction	35

3.5 GFP-Tef1p sub-domain localization and effects on the actin cytoskeleton	38
3.6 Modulation of Tef1p::Rho1p interaction	45
3.7 Tef1p effect on vacuole membrane fusion	52
CHAPTER 4 DISCUSSION	57
4.1 Tef1p is not a downstream effector molecule of Rho1p	58
4.2 Rho1p-interacting domain of Tef1p	59
4.3 Involvement of Calcium/Calmodulin on the Tef1p:Rho1p interaction	60
4.4 Potential roles for Tef1p in Rho1p activation and membrane fusion	61
CHAPTER 5 FUTURE DIRECTIONS	65
CHAPTER 6 CONCLUSIONS	68
CHAPTER 7 REFERENCES	70
APPENDIX A	76
APPENDIX B	77

LIST OF TABLES

Table 2-1	Oligonucleotides	13
Table 2-2	Plasmids	14
Table 2-3	Antibodies	14
Table 2-4	Drugs	15
Table 2-5	Bacterial Strains	15
Table 2-6	Yeast Strains	16

LIST OF FIGURES

Figure 1. Working model for distinct steps in membrane fusion	3
Figure 2. Identification of Tef1p as a novel vacuolar Rho1p binding protein	10
Figure 3. Tef1p and not other components of translation elongation machinery associate with vacuoles	30
Figure 4. Actin bundling activity of Tef1p is not necessary for vacuole localization	33
Figure 5. Tef1p:GDP and Rho1p:GDP are the preferred nucleotide states for interaction	36
Figure 6. Rho1p-binding domains of Tef1p	37
Figure 7. Actin cytoskeleton morphology and GFP-Tef1p sub-domain localization	39
Figure 8. Vacuole morphology and GFP-Tef1p sub-domain localization	42
Figure 9. Effect of GFP-Tef1p full-length and sub-domain expression on growth rates of wild-type and HA-RHO1 overexpressing yeast	46
Figure 10. Effects of calcium/calmodulin on Tef1p::Rho1p interaction	47
Figure 11. Effects of Tef5p, the guanine nucleotide exchange factor (GEF) of Tef1p, on Tef1p::Rho1p interaction	51
Figure 12. Effect of narciclasine, a GTPase targeting drug, on Tef1p::Rho1p interaction	53
Figure 13. Effects of Tef1p, Tef5p, narciclasine, and W7 on membrane fusion	54
Figure 14. Model of Tef1p - Rho1p function in vacuole fusion	63

CHAPTER 1

INTRODUCTION

1.1 Membrane Fusion

One of the defining characteristics of eukaryotic cells is the presence of an endomembrane system. Much of the sorting and trafficking of lipids and proteins is vesicle-mediated and thus membrane transport and membrane fusion are necessary steps. We use a simplified model system involving *Saccharomyces cerevisiae* (yeast) vacuoles to study the mechanisms of membrane fusion. The yeast vacuole model has been used extensively to define the roles of many of the proteins involved in trafficking and the fusion machinery (Wickner and Haas, 2000). Vacuole membrane fusion occurs in three distinct sub-reactions: priming, tethering, and fusion (**Fig. 1**). Priming is an ATP-dependent step, whereby Sec18p (N-ethylmaleimide soluble factor or NSF) binds to SNARE-associated Sec17p (soluble NSF-attachment protein or SNAP) to dissociate *cis*-SNARE complex proteins, freeing the t-SNARE Vam3p from Vam7p (*s*-SNARE) and Nyv1p, Vti1p and Ykt6p (*v*-SNAREs)(Ungerman et al., 1998; Price et al., 2000.). LMA1 is transferred from Sec18p to Vam3p to prevent reoccurrence of *cis*-SNARE pairing (Xu, et al. 1998). During priming Ypt7p (Rab GTPase) is also recruited to the vacuole. During docking an initial tethering event occurs between the Rab GTPase Ypt7p, and its effector complex, which leads to the reversible interaction between SNAREs on opposing membranes (*trans*-SNAREs). Once *trans*-SNARE pairs are stabilized, docking becomes irreversible (Ungerman et al., 1998). Fusion is the final and perhaps least understood stage in membrane fusion where the lipid bilayers of the opposing membranes are

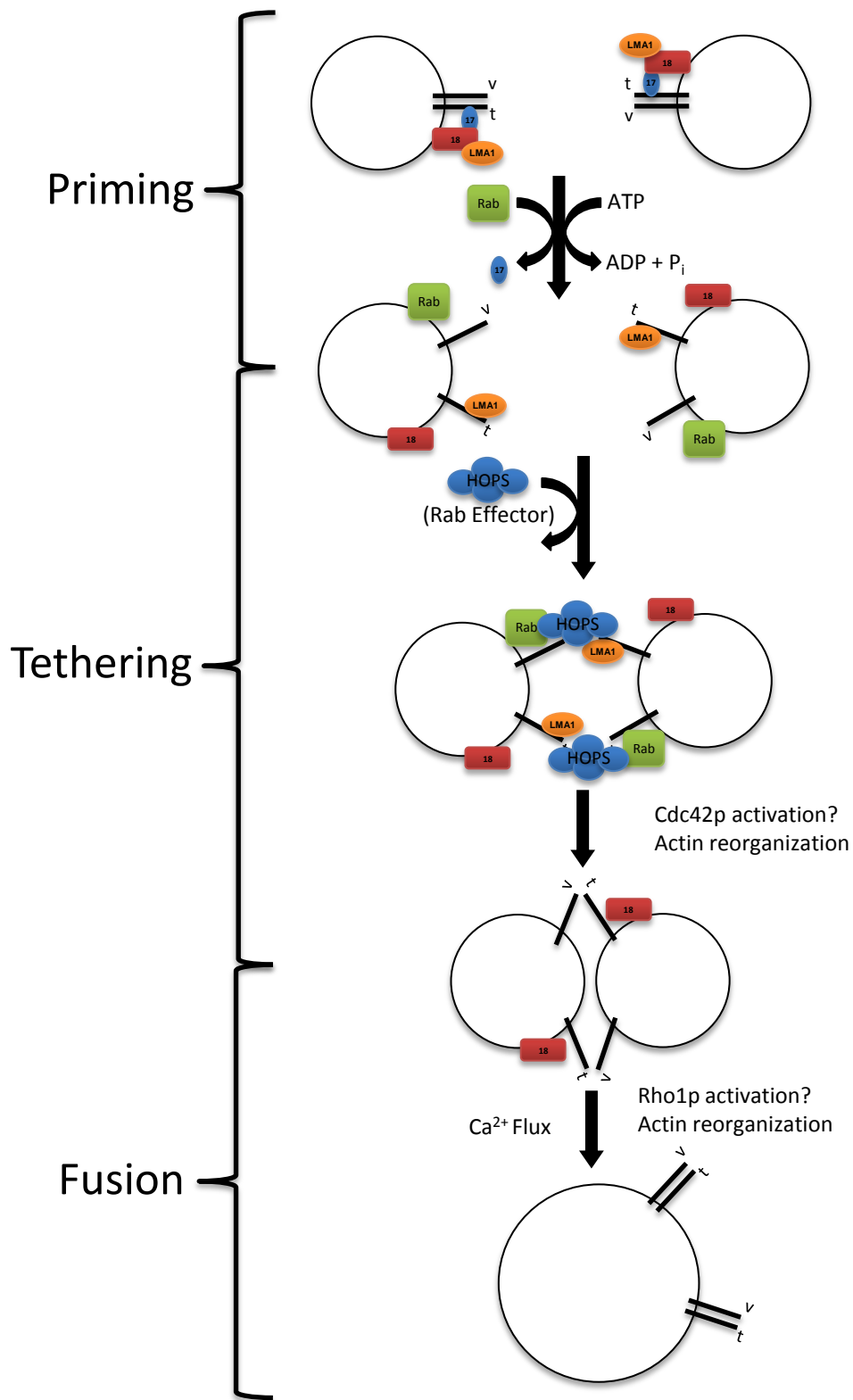


Figure 1. Working model for the distinct steps in membrane fusion. Adapted from Ungermann et al. 1998. See *INTRODUCTION* for a description of the model.

fused and the luminal contents can then mix. One of the final steps that occurs is calcium flux that leads to activation of calmodulin and unknown downstream effects (Peters and Mayer, 1998).

1.2 Actin Dynamics

The actin cytoskeleton is a highly dynamic series of structures that have roles in many physiological processes from organelle inheritance to cytokinesis (Mosely and Goode, 2006). Actin exists as a monomeric 42 kDa protein (encoded by a single gene in *S. cerevisiae*, *ACT1*), as well as polymeric double helical filaments. The two states exist in dynamic equilibrium that can be altered by affecting the rates of polymerization versus depolymerization (Mosely and Goode, 2006). An example of a process in which both actin depolymerization *and* polymerization are required is that of exocytosis. The cortical actin network acts as a physical barrier that must be broken down in order to allow access for contact between vesicles and the plasma membranes lipids (Eitzen et al., 2002; Eitzen, 2003). Actin polymerization is then required to complete membrane fusion (**Fig. 1**), likely through positional restriction of lipids and the fusion machinery (Malacombe et al., 2006). The initial nucleation of actin filaments is slow as small oligomeric actin filaments are unstable. However, once an actin filament is established, it can enter a steady state of “treadmilling” where the barbed end growth rate is equal to the rate of the pointed end depolymerization (Mosely and Goode, 2006). Several signaling molecules, such as the Rho-family of GTPases, have

been identified that are able to induce actin nucleation and modify the polymerization rate (Jaffe and Hall, 2005), while modulators of the rate of depolymerization have been identified but are less understood (Brieher, 2013). The Rho family of GTPases are known to govern both the activation of the actin remodeling machinery as well as define the subcellular localization of these events.

1.3 Rho GTPases

Rho GTPases are a family of proteins that are known to be involved in actin reorganization (Hall, 1998). Mammalian cells contain three classes of Rho GTPases, Rho, Rac, and Cdc42, while yeast have two, Rho and Cdc42p. Rho GTPases switch between two states, a GTP-bound “on”-state or a GDP-bound “off”-state. The conversion between the two states is controlled by guanine nucleotide exchange factors or GEFs and GTPase activating proteins or GAPs (Jaffe and Hall, 2005). GEFs are able to destabilize the interaction between the GDP nucleotide and Rho protein by disturbing the coordination of Mg^{2+} , which is required for nucleotide binding to Rho, causing dissociation of GDP and allowing GTP binding thus switching the Rho GTPase to its “on” conformation (Zhang et al., 2000). The intrinsic rate of GTP hydrolysis is relatively slow for Rho GTPases and thus GAPs are required to activate GTPase activity leading to the hydrolysis of GTP, placing the RhoGTPase in a GDP-bound “off”-state. GAPs achieve this by coordinating the Switch I and II regions of the GTPase domain of Rho GTPases leading to an increased

rate of hydrolysis (Gamblin and Smerdon, 1998). It is the same Switch I region that is also believed to be responsible for binding to downstream effectors. When Rho GTPases are in their GDP-bound state, the Switch I region occupies a “closed” conformation making it unavailable for effector binding. Upon GTP binding, the Switch I region is made available for effector binding (Sahai et al., 1998).

Two Rho GTPases are involved in vacuole fusion in *S. cerevisiae*, Rho1p and Cdc42p (Eitzen et al., 2001), and have previously been shown by the Eitzen lab to be sequentially activated during membrane fusion with Cdc42p activation occurring before Rho1p (Jones et al., 2010, Logan et al., 2010). While activation of both Rho1p and Cdc42p is known to lead to increased actin polymerization, they act through differing effector proteins. In the case of Cdc42p, activation leads to a downstream signaling cascade through WAVE and WASP (Las17 and Vrp1p in *S. cerevisiae*) to activate the Arp2/3p pathway. Arp2/3p activity nucleates branched actin networks (Jaffe and Hall, 2005). Rho1p activation leads to downstream signaling that activates formins (Bni1p and Bnr1p in the case of *S. cerevisiae*). Formins act by inducing nucleation and subsequently adding monomeric actin/cofilin complexes to the barbed end of the actin filament, creating long un-branched filaments (Zigmond, 2004). With regards to membrane fusion, actin remodeling (both depolymerization and polymerization) has been shown to be a necessary step as both stabilizing and destabilizing F-actin using the drugs jasplakinolide and latrunculin respectively, inhibits membrane fusion

(Eitzen et al., 2002). Cdc42p has previously been shown to be responsible for the actin polymerization step in membrane fusion (Isgandarova et al., 2007). The role of Rho1p, while necessary for membrane fusion, has yet to be further defined.

1.4 Translation Elongation Factor 1A: Tef1p

Tef1p (also known as Elongation Factor 1 α , EF1 α , or EF1A in humans) is a dual function protein with roles in both protein translation and actin cytoskeleton organization. Here, I describe each of these functions and how they are coordinated by regulators of Tef1p. Previously, Tef1p has been shown to interact with formin proteins (Bni1p) which are downstream effectors of Rho1p (Umikawa et al., 1998). We will now present evidence that Tef1p interacts directly with Rho1p.

1.4.1 The canonical role of Tef1p in protein translation

Tef1p is a ~50 kDa GTPase that has a well characterized function in protein translation. Tef1p is an aminoacyl-tRNA transferase that, when GTP-bound, forms a complex with aminoacylated-tRNAs and shuttles them to the ribosome. When the tRNA interacts with its appropriate codon at the ribosome, the GTPase activity of Tef1p is activated and upon conversion to Tef1p:GDP, Tef1p is released from the ribosome (Andersen et al., 2003). Tef1p is composed of three distinct domains. Domain 1 is composed of a conserved GTPase domain. Domain 2 is responsible for aminoacyl-tRNA

binding. Domain 3 has been shown to have actin binding properties, while all three domains have affinity for calcium/calmodulin (Morita et al., 2008).

1.4.2 Actin bundling properties of Tef1p

Tef1p was first identified as an actin binding protein in 1990 when a ~50 kDa actin binding protein then called ABP-50 was sequenced in *Dyctostelium* (Yang et al., 1990). The actin binding properties of Tef1p have since been implicated in translation where mutants of Tef1p lacking actin binding properties have protein initiation defects (Gross and Kinzy, 2007). Interestingly, overexpression of Tef1p does not appear to have an effect on protein translation, but causes growth defects due to improper organization of the actin cytoskeleton (Munshi et al., 2001). eEF1B or Tef5p, which functions as a GEF for Tef1p, has been shown to disrupt the actin binding activities of Tef1p, suggesting that the exchange of GDP for GTP on Tef1p may functionally switch Tef1p from an actin bundling role into a translational role (Pittman et al., 2009). Tef1p was shown to bundle actin filaments into higher order, square-packed cable structures (Owen et al., 1992; Munshi et al., 2001). The nature of this binding order suggests that Tef1p occludes additional actin binding proteins and stabilizes long unbranched filaments (Owen et al., 1992).

Further evidence of Tef1p having a functional role in actin organization independent of translation was found when Tef1p was identified as binding to Bni1p, a Rho1p effector (Umikawa et al., 1998).

Umikawa et al. were able to show that the Tef1p binding domain of Bni1p was necessary for the function of Bni1p, but that Bni1p in fact inhibited the actin binding properties of Tef1p (Umikawa et al., 1998). Narciclasine is a small molecule drug that has been shown to directly bind to Tef1p and inhibit Tef1p actin bundling activity while also activating Rho1p, though through an unknown mechanism (Van Goitsenoven et al., 2010; Lefranc et al., 2012).

1.5 Focus and goals of this thesis

Recently, the Eitzen lab identified a vacuolar Rho1p interacting protein as Tef1p (**Fig. 2**). The goal of this thesis work was to identify the Rho1p-interacting domain of Tef1p as well as specific conditions of Rho1p:Tef1p binding. Tef1p was shown to stably associate with the vacuole membrane and therefore we decided to focus on the potential functional significance of the Tef1p:Rho1p interaction with regards to effects on membrane fusion.

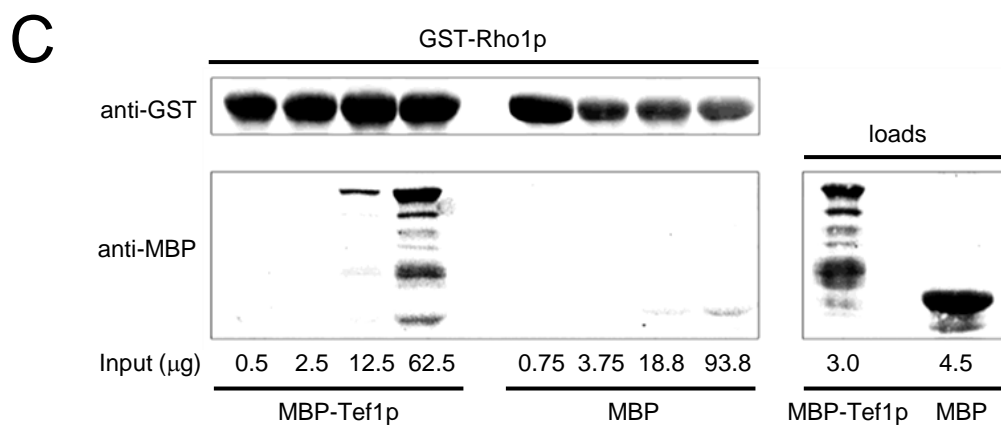
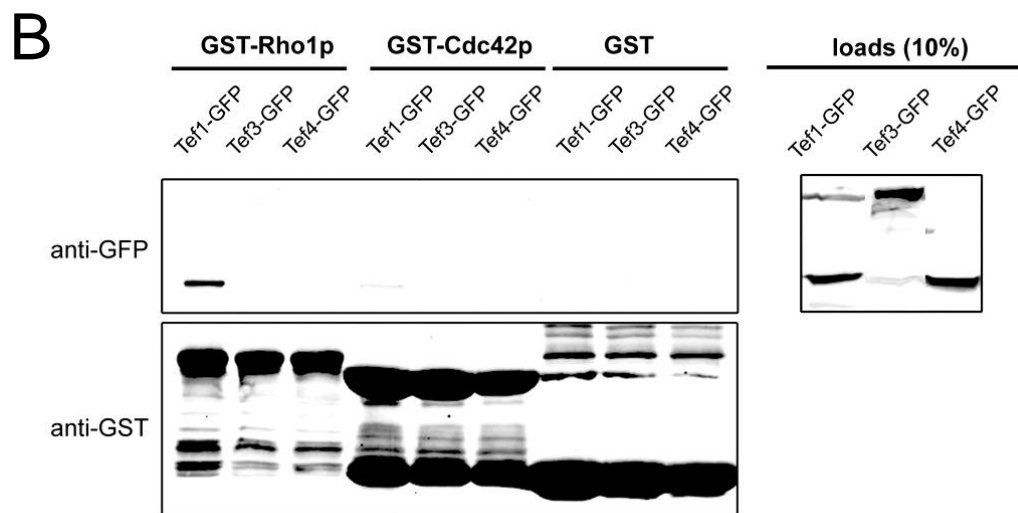
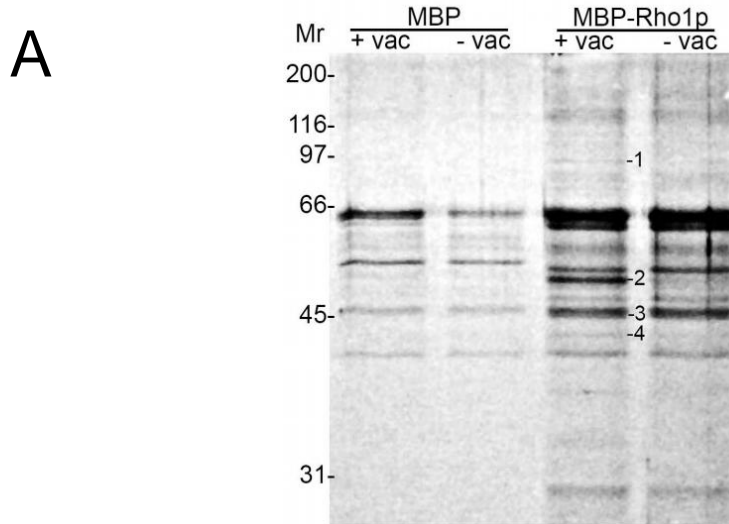


Figure 2. Identification of Tef1p as a novel vacuolar Rho1p binding protein. (A) Vacuoles, isolated from strain KTY1, were primed for fusion by incubation in fusion reaction buffer and 0.5 mg/ml cytosol. After a 30 min incubation vacuoles were reisolated by centrifugation, washed twice in fusion reaction buffer and solubilized by adding Triton-X100 to 0.5% (v/v). Solubilized vacuoles were incubated with MBP or MBP-Rho1p bound to amylose resin. Resin-bound proteins were examined by SDS-PAGE and silver staining. Several unique MBP-Rho1p-associated bands were identified by mass spectroscopy: 1. Fks1p, 2. Tef1p, 3. MBP, 4. ribosomal subunit 10 (performed by G. Eitzen). (B) Lysates from *S. cerevisiae* expressing GFP-tagged Tef1p, Tef3p, or Tef4p (chromosomal C-terminal integration) were incubated with glutathione resin-bound GST-Rho1p, GST-Cdc42p or GST. Bound proteins were analyzed by SDS-PAGE and immunoblot (performed by M. Logan). (C) Direct interaction between Rho1p and Tef1p. GST-Rho1p was immobilized on glutathione beads and incubated with increasing amounts of MBP-Tef1p or MBP purified from *E. coli* lysate (performed by Y. Yang).

CHAPTER 2

MATERIALS AND METHODS

2.1 Oligonucleotides

All oligonucleotides purchased from Integrated DNA Technologies

Table 2-1 Oligonucleotides

Name	Sequence	Application
TEF1-rec1	GAA TTC GAT ATC AAG CTT ATC GAT	pGREG-576-TEF1 FL,
	ACC GTC GAC AAT GGG TAA AGA GAA	pGREG-576-TEF1 D1,
	GTC TCA CA	pGREG-576-TEF1 D12
TEF1-rec2	GCG TGA CAT AAC TAA TTA CAT GAC	pGREG-576-TEF1 FL
	TCG AGG TCG ACT TAT TTC TTA GCA	pGREG-576-TEF1 D3
	GCC TTT TGA	pGREG-576-TEF1 D23
TEF1 D1-rec2	GCG TGA CAT AAC TAA TTA CAT GAC	pGREG-576-TEF1 D1
	TCG AGG TCG ACT TAT CTA GAT GGT	
	TGT TCA ATG	
TEF1 D2-rec1	GAA TTC GAT ATC AAG CTT ATC GAT	pGREG-576-TEF1 D2
	ACC GTC GAC ACC AAC TGA CAA GCC	pGREG-576-TEF1 D23
	ATT GAG	
TEF1 D2-rec2	GCG TGA CAT AAC TAA TTA CAT GAC	pGREG-576-TEF1 D2
	TCG AGG TCG ACT TAT GGA TCG TTC	pGREG-576-TEF1 D12
	TTA GCG TCA C	
TEF1 D3-rec1	GAA TTC GAT ATC AAG CTT ATC GAT	pGREG-576-TEF1 D3
	ACC GTC GAC ACC AAA GGG TTG CGC	
	TTC TTT	

2.2 Plasmids

Table 2-2 Plasmids

Plasmid	Selection	Source
pGREG576	URA3	Jansen et al. (2004)
pGEX-4T1	ampicillin	Amersham Biosciences

2.3 Antibodies

Table 2-3 Antibodies

Antibody	Source	Host	Type	Working Dilution
α -GFP	<i>Eitzen</i>	Rabbit	Polyclonal	1:1000
α -GFP	<i>Berthiaume</i>	Rabbit	Polyclonal	1:1000
α -GST	<i>Sigma</i>	Mouse	Monoclonal	1:10,000
α -calmodulin	<i>Wickner</i>	Rabbit	Polyclonal	1:2000
α -actin	<i>Eitzen</i>	Rabbit	Polyclonal	1:1000

2.4 Drugs

Table 2-4 Drugs

Name	Target	Source	Reference
narciclasine	Tef1p	Tocris Biosciences	Van Goietsenoven et al. (2010)
W7	Calmodulin	Tocris Biosciences	Hiyashi et al., (1980)
Lat B	Actin	BioMol	Spector et al., (1983)

2.5 Microorganism Strains and Growth Conditions

2.5.1 Bacterial Strains

Table 2-5 Bacterial strains

Strain	Genotype	Reference
DH5 α	<i>F⁻, -ϕ80lacZΔM15, Δ(lacZYA-argF), U169, recA1, endA1, hsdR17(<i>rk⁻, mk⁺</i>), phoA, supE44, thi-1, gyrA96, relA1 λ</i>	Invitrogen
Rosetta TM	<i>F⁻, ompT, hsdS_B(<i>r_B⁻, m_B⁻</i>), gal, dcm, met</i> pRARE (tRNAs for AGG, AGA, AUA, CUA, CCC, GGA codons on a compatible chloramphenicol-resistant plasmid)	Invitrogen

2.5.2 Yeast Strains

Table 2-6 Yeast Strains

Strain	Genotype	Reference
BY4742	<i>MATa, his3d1, leu2d0, lys2d0, ura3d0</i>	
BJ5459	<i>Mata, pep4::HIS3, prb1-Δ1.6R, his3, leu2, ura3, lys2, trp1, can1</i>	
KTY1	<i>Mata, pep4::kanMX, prb1::LEU2, his3, leu2, ura3, lys2</i>	
KTY2	<i>Mata, pho8::kanMX, his3, leu2, ura3, lys2</i>	
TEF1-GFP	<i>Mata, hisd31, leud0, met15d0, ura3d0, tef1::TEF1-GFP</i>	
HA-RH01	<i>Mata, pep4::kanMX, prb1::LEU2, his3, leu2, ura3, lys2 HIS3-P_{GAL}-3HA::RH01</i>	
K91-1A	<i>Mata, pho8::AL13, pho13::pPH13, his3, ura3, lys2</i>	

2.6 Transformation of microorganisms

2.6.1 Bacterial Transformation

Bacteria were transformed with plasmid DNA as per Invitrogen

DH5α subcloning efficient cells transformation protocol. Briefly, 50 μl DH5α

cells were thawed on ice and 1 μl of plasmid DNA was added. The mixture

was incubated on ice for 30 min then heat shocked at 42°C for 20-25 s then placed back on ice for 2 min. Cells were then directly plated onto LB_{amp} plates. If transformation efficiency was low, 1 ml of pre-warmed LB was added and cells were incubated for 1 h at 37°C before being spun down and suspended in 50-100 µl sterile water and plated on LB_{amp} plates.

2.6.2 Lithium Acetate Yeast Transformation

Yeast transformation was performed as per Geitz and Shiestl (1996) with modifications. Yeast were inoculated into 2-5 ml of YPD and grown at 30°C to an OD₆₀₀ of 1.0-2.0. Cells were harvested by centrifuging 15 s at 20,000 x *g*, washed once with sterile water and washed once with 100 mM lithium acetate. The transformation mixture of 240 µl 50% (wt/vol) polyethylene glycol 3350, 36 µl 1 M lithium acetate, 25 µl of 2.0 mg/ml denatured salmon sperm-DNA and 50 µl water/DNA (plasmid and/or PCR product) was layered stepwise. The transformation mixture was vortexed until pellet was completely dissolved and incubated 30°C for 30 min and heat shocked at 42°C for 20-25 min. Cells were recovered by centrifugation 7000 x *g* for 15 s. The transformation mixture was removed with a micropipette. The pellet was suspended in 50-100 ml of sterile water and plated onto appropriate complete synthetic medium (e.g. lacking uracil, CSM-ura) media. Transformations were confirmed by protein expression using western blot and microscopy.

2.7 Protein expression, lysate preparation, and protein purification

2.7.1 Bacterial protein expression and lysate preparation

For protein expression in bacteria, 100 ml of LB_{amp} or LB_{amp/chloroamp} were inoculated and grown overnight in a 37°C shaking incubator at 190 RPM. The overnight culture was added to 1 L of LB_{amp} or LB_{amp/chloroamp} and grown for 3-4 h. IPTG was added to 1 mM for induction of the P_{Tac} inducible promoter. Cells were harvested by centrifugation 10 min at 5000 x *g*, washed once in distilled water, and 0.5-1 ml of 60X protease inhibitor cocktail (60X PIC: 10 µg/ml leupeptin, 25 µg/ml pepstatin, 12.5 mM 1,10 -phenanthroline, 5 mM Pefabloc) was added before freezing cells at -80°C. Cells were suspended in lysis buffer (20 mM HEPES, pH 7.5, 100 mM NaCl, 0.1 mM DTT, 0.1 mM phenylmethylsulfonyl fluoride (PMSF). 1XPIC). Cells were lysed by running the suspension through an Avestin Emulsiflex C-3 for 5 min at 15,000 PSI. After emulsification, Triton X-100 was added to 0.5% (v/v) and the emulsion was centrifuged for 45 min at 4°C and 30,000 x *g*. The supernatant was collected and the total protein concentration was determined by Bradford assay (Bradford, 1976).

2.7.2 Yeast protein expression and lysate preparation

100 ml CSM-ura were inoculated and incubated overnight in a 30°C shaking incubator. The overnight culture was added to 1 L YPDG_{kan} and grown for a further 4-6 h. Cells were harvested by centrifugation for 10 min at 5000 x *g*.

Cells were washed once in distilled water, and 0.5-1 ml of 60X PIC was added before freezing cells at -80°C. Cells were suspended in lysis buffer (20 mM HEPES, pH 7.5, 100 mM NaCl, 0.1 mM DTT, 0.1 mM PMSF, 1XPIC, 10% (v/v) glycerol). Cells were lysed by running the suspension through an Avestin Emulsiflex C-3 for 5 min at 25,000 PSI. After emulsification, Triton X-100 was added to 0.5% (v/v), and emulsion was centrifuged for 45 min at 4°C and 30,000 *x g* and supernatant is collected. Total protein concentration of the lysate concentration was determined by Bradford assay (Bradford, 1976).

2.7.3 Protein purification

2.7.3.1 GST-fusion protein purification

1 ml glutathione-sepharose resin (Pharmacia) is placed in a 5 ml disposable polypropylene column (Pierce) and equilibrated in H-Buffer (20 mM HEPES ,pH 7.5, 100 mM NaCl, 0.1 mM DTT, 0.1 mM phenylmethylsulfonyl fluoride (PMSF), 1XPIC, 0.5% (v/v) Triton X-100). Pre-cleared lysates prepared as described in Section 2.7.1 are ran over the column and followed by three washes with H-Buffer. Protein was eluted using H-Buffer with 10 mM reduced glutathione (Sigma). Fractions of three to five drops are collected and traces of protein are detected by Bradford assay (Bradford, 1976). Fractions with detectable levels of protein were pooled and the final protein concentration was assayed by Bradford assay (Bradford, 1976).

2.7.3.2 MBP-fusion protein purification

1 ml amylose resin (New England Biolabs) is placed in a 5 ml disposable polypropylene column (Pierce) and equilibrated in H-Buffer (20 mM HEPES, pH 7.5, 100 mM NaCl, 0.1 mM DTT, 0.1 mM phenylmethylsulfonyl fluoride (PMSF), 1XPIC, 0.5% (v/v) Triton X-100). Pre-cleared lysates prepared as described in Section 2.7.1 are ran over the column and followed by three washes with H-Buffer. Protein was eluted using H-Buffer with 10 mM maltose (Sigma). Fractions of three to five drops are collected and traces of protein are detected by Bradford assay (Bradford, 1976). If protein is to be used in membrane fusion experiments, Triton X-100 was omitted and protein was subjected to buffer exchange into PS buffer using a G25 column (GE Healthcare).

2.8 Yeast vacuole membrane preparation

Yeast vacuoles were isolated essentially as described by Haas (1995) with some modifications. 1L culture of yeast strain of choice was grown overnight at 30°C to an OD₆₀₀ of 1.3. Cells were harvested by centrifugation at 5000 RPM for 5 min using a Beckman JLA 10.500 rotor. Cells were suspended in a solution of 100 mM Tris-Cl, pH 9.0, and 10 mM DTT then incubated for 15 min at 30°C with occasional vortexing. Cells were then spun down again and suspended in 15 ml spheroplasting buffer (12 ml 0.2% YPD, 2.25 ml 4 M sorbitol, 0.75 ml 1 M potassium phosphate, pH 7.5, 2 ml lyticase solution) and incubated for 45 min at 30°C, with occasional vortexing. Cells were spun

down with slow acceleration from 3000-5200 RPM over 2 min followed by 4 min at 5200 RPM in a JA 25.50 rotor at 3°C. The supernatant was carefully aspirated since the pellets were fairly loose. Spheroplasted cells were then suspended in 2.5 ml of 15% (wt/v) ficoll solution (15% (wt/v) ficoll, 20 mM PIPES pH 6.8, 200 mM sorbitol). Cells were then incubated with 200 µl of dextran solution (1 mg DEAE Dextran dissolved in 1 ml 15% (wt/v) ficoll solution) for 5 min on ice, then for 5 min at 30°C then placed back on ice. The suspension was placed at the bottom of an SW41 tube. This was overlaid with 2.5 ml of 8% (wt/v) ficoll solution, and then 2.5-3.0 ml 4% (wt/v) ficoll solution to approximately 1 cm below the rim of the tube. The remainder of the tube was filled with 0% (wt/v) ficoll solution (20 mM PIPES pH 6.8, 200 mM sorbitol) to approximately 3 mm from the top. The gradient as then centrifuged at 32,000 RPM in an SW41 rotor for 2 h at 4°C. Vacuoles were recovered from the interface between the 0% and 4% layers with a P200 pipet with 3 mm of the tip cut off. Vacuole concentration was determined by Bradford assay (Bradford, 1976).

2.9 Biochemical assays

2.9.1 Affinity pulldown

15 µl per reaction glutathione-sepharose resin (Pharmacia) were pre-equilibrated in H-Buffer (20 mM HEPES, pH 7.5, 100 mM NaCl, 0.5% (v/v) Triton X-100, 0.1 mM dithiothreitol (DTT), 0.1 mM PMSF, 1X PIC), and 750 µg of GST-tagged bait protein were incubated in H-Buffer for 15 min at 4°C.

The resin was then washed three times with H-Buffer, and 2-10 mg of target protein lysate was incubated for 90 min at 4°C. The bead was then washed times with H-Buffer and suspended in 1.2X SSB Buffer (72 mM Tris-Cl, pH 6.8, 2.4% SDS, 12% glycerol, 6% β -mercaptoethanol, 0.012% bromophenol blue) and boiled 5 min at 95°C before being analyzed by SDS-PAGE and western blot.

2.9.1.1 Chemical nucleotide exchange

GST-Rho1p was bound to glutathione resin and washed three times in H-buffer without $MgCl_2$. EDTA was added to 3 mM, and $GTP\gamma S$ or GDP was added to 40 μM . Samples were incubated for 5 min at 30°C with frequent mixing. $MgCl_2$ was added to 10 mM. The resin was washed three times with H-buffer (containing 5 mM $MgCl_2$) before incubation with yeast lysates. Tef1p-GFP target lysates were nucleotide-locked by adding EDTA to 3 mM and $GTP\gamma S$ or GDP to 40 μM . Lysates were incubated for 5 min at 30°C with frequent mixing. $MgCl_2$ was then added to 10 mM.

2.9.1.2 Quantification of binding

Western blots were scanned using a Li-Cor Odyssey imaging system. Bands of both GST-Rho1p or MBP-Rho1p and Tef1p-GFP protein were quantified using densitometry software in Odyssey v1.2. Tef1p-GFP band levels were normalized by dividing by 10% load band. These values were then divided by their corresponding GST/GST-Rho1p or MBP/MBP-Rho1p band value. Non-

specific binding of Tef1p-GFP to GST/MBP was deducted from the specific binding values. 100% Binding was set as the binding when no additional protein or drug was added to the binding reaction.

2.9.2 Co-immunoprecipitation

15 μ l per reaction of Protein A sepharose resin (Pierce) were washed three times with phosphate buffered saline (PBS). Three bead volumes of raw serum were added and 10X PBS was added to a final concentration of 1X PBS. 1X PBS was added to make the final volume to 1 ml, and tubes were placed in a nutator for 60 min at 4°C. Beads were washed two times in PBS and then two times in 100 mM HEPES, pH 8.8. Beads were then suspended in 100 mM HEPES pH 8.8, 20 mM dimethyl pimelimidate (DMP) and nutated for 60 min at 4°C. The cross-linking reaction was stopped by washing the beads in 200 mM ethanolamine, pH 8.0, and nutating for 2 h at room temperature. Beads were then washed three times in PBS and were used within 2 weeks. Prior to use the beads were pre-stripped by washing with 100 mM glycine pH 2.5 followed by three washes in H-Buffer. Enough lysate for two co-IPs was added to 15 μ l of normal IgG beads (non-specific) and nutated for 30 min at 4°C. Beads were recovered by centrifugation for 2 min at 2655 *g*. 1 mg of precleared lysate was added to 15 μ l of specific bead and nutated for 2 h at 4°C. After immunoprecipitation, the beads were recovered by centrifugation for 2 min at 2655 *g* and then washed three times with H-Buffer. Beads were eluted using 40 μ l 2X SSB without β -mercaptoethanol, vortexed for 5 s and

incubated at room temperature for 2 min. Beads were precipitated by centrifugation for 2 min at 2655 *g*. 25 μ l of the eluate was drawn off without disrupting the beads, and 25 μ l of 10% β -mercaptoethanol were added before boiling sample for 5 min at 95°C. Co-immunoprecipitated proteins were analyzed via SDS-PAGE and western blot.

2.9.3 Vacuole fusion assays

Vacuole fusion assays were performed essentially as described by Haas (1995). 3.5 μ g each of isolated vacuoles from KTY1 and KTY2 strains were mixed in fusion reaction buffer (FRB) in the presence of cytosol and/or test substances as indicated. Fusion reactions were incubated for 90 min at 27°C. Levels of matured alkaline phosphatase are assayed and are indicative of the level of membrane fusion.

2.10 Microscopy

2.10.1 Yeast live whole-cell wide-field microscopy

2 ml of minimal medium with 2% (wt/v) dextrose were inoculated with the required strains. 200 μ l of overnight culture were used to re-inoculate 1 ml of YPD_{kan} to induce expression of protein constructs. Strains were incubated for 3 h at 30°C. 300 μ l of this culture were taken, and vacuoles were stained with 1 μ l of 4 mM FM4-64 (Invitrogen). Cells were then spun down 15 s at 2655 *g* and suspended in 300 μ l of YPD and incubated for 30 min at 30°C. Cells were then spun down 15 s at 2655 *g* and submitted to a water shock in

300 μ l of doubly distilled water to induce vacuole fusion. 4 μ l were placed on a slide, and images were captured using a CoolSnap HQ camera and ImageJ software on a Zeiss Axioplan 2 at 100X/1.40N.A. objective and processed in Adobe Photoshop.

2.10.2 Yeast fixed whole-cell wide-field microscopy

Yeast strains were grown overnight in YP with 2% (wt/v) raffinose and 50 μ g/ml kanamycin (YPR_{kan}). 200 μ l of overnight culture were used to inoculate 3 ml of YP with 2% (wt/v) galactose and 50 μ g/ml kanamycin (YPG_{kan}) to induce expression of protein constructs. Cells were incubated for 3 h at 30°C. Cells were harvested by centrifugation at 1000 *g* for 15 s. Cells were washed in 3.7% Formaldehyde solution then fixed at room temperature for 1 h in 3.7% formaldehyde solution. Cells were washed twice in PBS and suspended in 20 μ l of PBS. 1 μ l of fluorescently labeled Alexa Fluor 546-phalloidin (Molecular Probes) was added to the 20 μ l suspension and incubated in darkness for 1 h at 30°C. Cells were washed three times with PBS and suspended in 20 μ l of Prolong Gold (Invitrogen) and mounted on a slide. Images were captured with an AxioCam MRm and Axiovision 4.8 software using a Zeiss Observer Z1 microscope with a 100X/1.40N.A. objective lens.

2.10.3 Yeast vacuole wide-field microscopy

300 μ l of vacuoles isolated via protocol in Section 2.8 were stained with 1 μ l of FM4-64 dye and either imaged immediately or aliquoted for exposure to drug. If drug was being used then the aliquot was incubated for 30 min at 30°C before 4 μ l were taken and placed on a slide for microscopy. Images were captured using a CoolSnap HQ camera and ImageJ software on a Zeiss Axioplan 2 at 100X/1.40N.A. objective and processed in Adobe Photoshop.

2.10.4 Yeast growth curves

2 ml of YP with 2% raffinose 50 μ g/ml kanamycin (YPR_{kan}) were inoculated with appropriate strains of yeast and incubated overnight at 30°C. 100 μ l of overnight culture were used to inoculate 4 ml of YP with 2% galactose and 50 μ g/ml kanamycin (YPG_{kan}) for induction of GFP-Tef1p domain constructs and/or 3xHA-Rho1p expression and incubated overnight at 30°C. OD₆₀₀ of cultures were measured and used to inoculate 1.5 ml of YPG_{kan} to a starting OD₆₀₀ of 0.05 in a 24 well clear bottom plate. The plate was placed in a BMG Labtech CLARIOstar platereader and incubated at 30°C. OD₆₀₀ was read every 10 min preceded by 1 min of shaking at 400 RPM. Doubling time was determined using CLARIOstar data analysis software where the maximal slope of a consecutive 12 point sample between 12 and 20 h was used and entered into the equation $f(x)=\ln(2)/x$; where $f(x)$ = the slope and x is the doubling time as derived from the doubling time formula $P = P_0(2^{t/x})$

CHAPTER 3

RESULTS

3.1 Identification of a vacuolar Tef1p::Rho1p interaction

The Eitzen lab has previously shown that two Rho family GTPases, Cdc42p and Rho1p, were necessary for vacuole fusion and are sequentially activated during membrane priming for fusion (Eitzen et al., 2001; Logan et al., 2011). Cdc42p shows rapid activation upon priming with Rho1p showing slower activation (Logan et al., 2011). While Cdc42p has been shown to be responsible for membrane-associated actin polymerization through the action of Arp2/3 (Isgandarova et al., 2009), the role of Rho1p in vacuole fusion has not been well defined. To investigate the role of Rho1p in vacuole fusion we wanted to identify vacuole-associated Rho1p binding partners. To do this, we primed vacuoles in fusion reaction buffer (FRB), before solubilizing and incubating with amylose resin-bound MBP (Maltose Binding Protein) or MPB-Rho1p. A uniquely associating ~50 kDa peptide was identified by mass spectroscopy as translation elongation factor 1 α , or Tef1p (**Fig. 2A**). Tef1p is the yeast homolog of eEF1A in humans that has a predominant role in protein synthesis where it shuttles aminoacylated-tRNA to the ribosome (Andersen et al., 2003). Interestingly, Tef1p has also been shown to bind actin and bundle actin filaments into large square-packed bundles (Munshi et al., 2001).

To determine the specificity of the interaction between Tef1p and Rho1p, *in vitro* pull-down assays were performed using GFP-tagged Tef1p, or other components of translation elongation machinery, Tef3p-GFP and Tef4p-GFP, which are yeast homologs of EF-1 γ (Kinzy et al., 1994). These

were incubated with immobilized GST-Rho1p, or the additional Rho family GTPase, GST-Cdc42p, to analyze specificity (**Fig. 2B**). Tef1p-GFP interacted specifically with GST-Rho1p and not GST-Cdc42p, while Tef3p-GFP and Tef4p-GFP bound to neither. MBP-Tef1p purified from *E. coli* lysate also showed binding to GST-Rho1p in a dose-dependent manner (**Fig. 2C**). These data indicate that the Tef1p:Rho1p interaction is direct and specific and may hold information about the differences in activation and activity between Rho1p and Cdc42p.

3.2 Tef1p is enriched on vacuole membranes

After the interaction of Tef1p with Rho1p was discovered, we investigated the sub-cellular localization of Tef1p to determine if there was a pool localized to vacuoles. Purified yeast vacuoles and whole lysate were prepared from strains expressing Tef1p-GFP, Tef2p-GFP, Tef3p-GFP, or Tef4p-GFP and analyzed by SDS-PAGE and immunoblot (**Fig. 3A**). Tef1p-GFP and Tef2p-GFP (identical homologues) were found to be enriched on vacuoles as compared with the other translation elongation factors Tef3p-GFP and Tef4p-GFP. Tef1p-GFP and Tef2p-GFP, which are 100% homologues, also showed slight enrichment over actin, which is known to be vacuole-associated (Isgandarova et al., 2007).

We then examined vacuole-association of Tef1p-GFP by microscopy. Vacuoles were isolated from strains expressing a vacuolar H⁺-ATPase Vma1p-GFP, Tef1p-GFP, Tef3p-GFP, or Tef4p-GFP, then stained with the

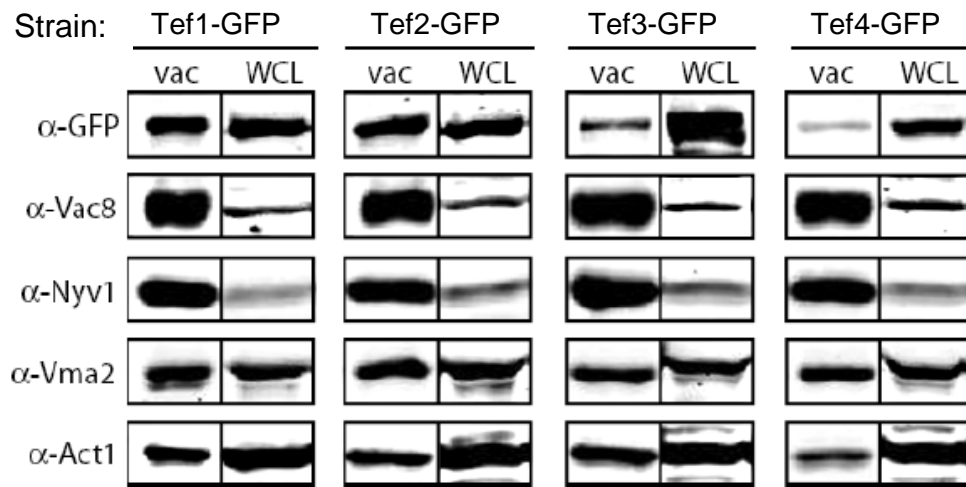
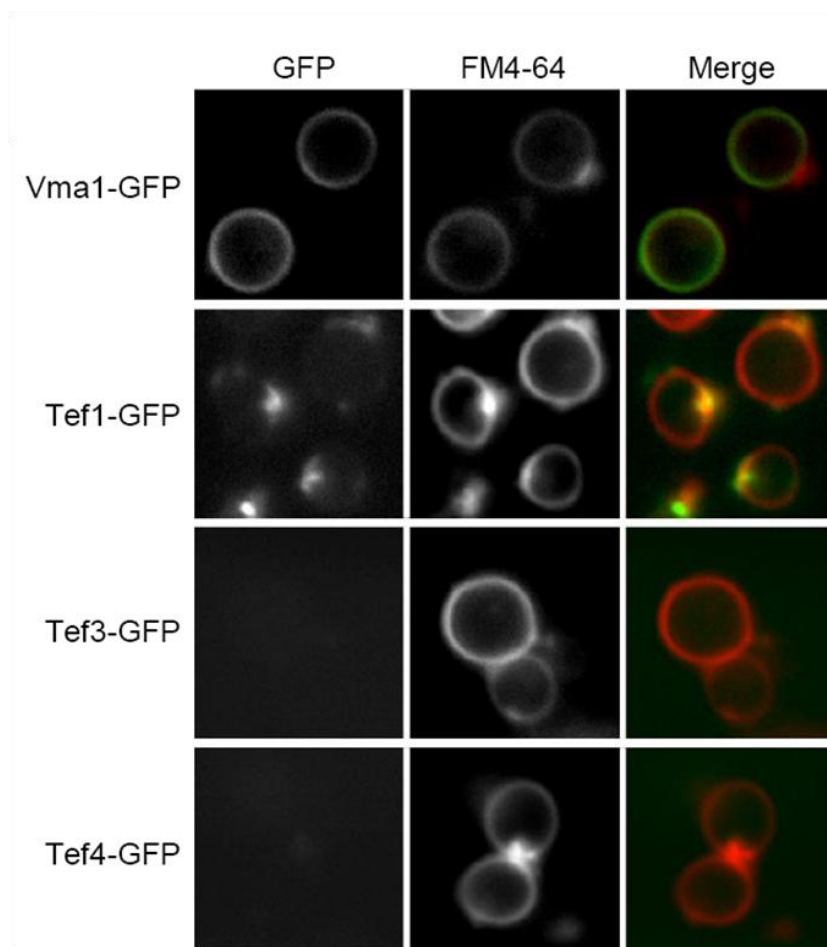
A**B**

Figure 3. Tef1p and not other components of the translation elongation machinery associate with vacuoles. (A) Whole cell lysate (WCL, 100 μ g) and purified vacuoles (vac, 10 μ g) isolated from *S. cerevisiae* strains expressing endogenously tagged Tef1p-GFP, Tef2p-GFP, Tef3p-GFP, and Tef4p-GFP were analyzed by SDS-PAGE and immunoblot. (B) Vacuoles isolated from *S. cerevisiae* expressing known vacuolar proteins Vma1p-GFP, Tef1p-GFP, Tef3p-GFP, Tef4p-GFP were stained with lipophilic dye FM4-64 and analyzed by wide-field fluorescence microscopy (performed by M. Logan).

lipophilic dye FM4-64 and imaged by fluorescence microscopy (**Fig. 3B**). Vma1p-GFP and Tef1p-GFP were found to localize to the vacuole membrane, while Tef3p-GFP and Tef4pGFP were not observed on the vacuole membrane. Interestingly, Tef1p-GFP appears to be present on the vacuole membrane in discrete foci, which may offer insight into the function of Tef1p on the vacuole membrane.

Next, we examined the effect of the drugs narciclasine and latrunculin B (Lat B) to determine the role of actin in vacuolar localization of Tef1p-GFP (**Fig. 4**). Narciclasine is a small molecule drug known to inhibit the actin bundling activity of Tef1p (Van Goietsenoven et al., 2010) while Lat B prevents F-actin formation through binding of actin monomers (Spector et al., 1983). In the absence of drug, we saw the typical single Tef1p-GFP puncta on each respective vacuole (**Fig. 4A, top panels**). Interestingly, when vacuoles were exposed to 500 nM narciclasine (**Fig. 4A, middle panels**), there appeared to be an increase in levels of Tef1p-GFP associated with the vacuole. If Tef1p-GFP localization was dependent on its actin binding activity, we would have expected to see a decrease in vacuole association in the presence of narciclasine. Additionally, when we expose the vacuoles to Lat B (**Fig. 4A, lower panels**), which should prevent the formation of filamentous actin and decrease the amount of Tef1p-GFP if actin binding is necessary for vacuole localization, we saw no change in the association of Tef1p-GFP with the vacuole. However, the Tef1p-GFP signal appeared to be more dispersed as opposed to discrete puncta, suggesting that while actin is not necessary for

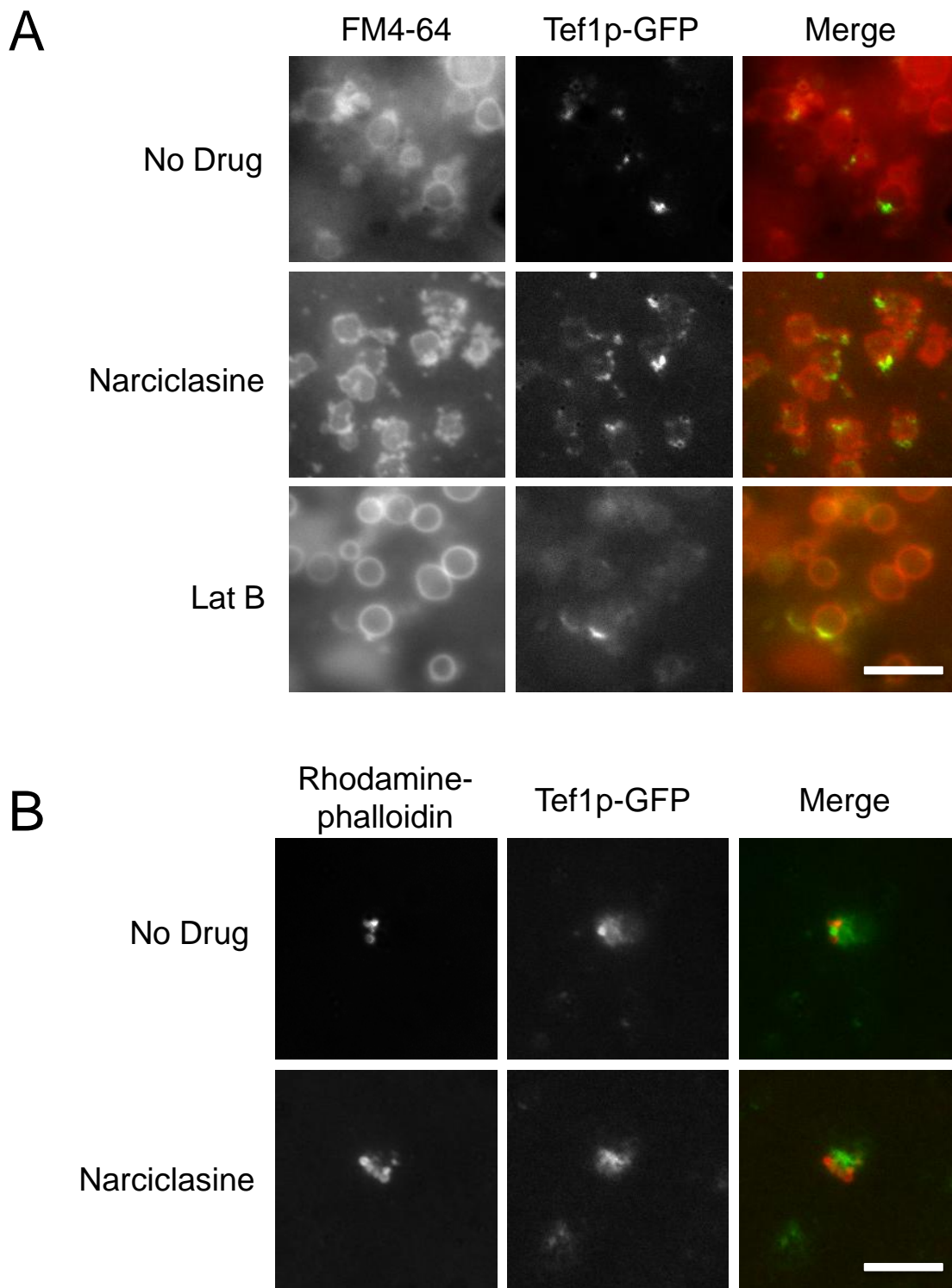


Figure 4. Actin bundling activity of Tef1p is not necessary for vacuole localization. Isolated yeast vacuoles were treated with 500 nM narciclasine or 10 μ M latrunculin B and stained with FM4-64 (A), or treated with 500 nM narciclasine and stained with rhodamine phalloidin (B). Vacuoles were then imaged by wide-field fluorescence microscopy. Bar = 5 μ m

Tef1p-GFP localization to the vacuole, it may be involved with specific subdomain localization on the vacuole. When we stained actin on vacuoles isolated from Tef1p-GFP expressing yeast using rhodamine phalloidin and expose the vacuoles to narciclasine, we observed little to no co-localization of actin with Tef1p-GFP (**Fig. 4B**). However, the two proteins appear to be restricted to similar areas of localization on the vacuole.

3.3 Nucleotide dependence of the Tef1p::Rho1p interaction.

An obvious area to investigate that could potentially offer some insight into the nature of the Tef1p::Rho1p interaction would be the nucleotide state of Tef1p and Rho1p in the interaction since they are both GTPases. We did not find any Tef1p amino acid sequences that resembled a Dbl homology-Pleckstrin homology (DH-PH) domain that is characteristic of RhoGEFs (Rossman et al., 2005; Aghazadeh, 1998). Thus, we hypothesized that Tef1p was a downstream effector of Rho1p. It has previously been shown that Rho effectors preferentially bind to Rho1p when it is in a GTP-bound state and this characteristic can also be used to assay the activation state of Rho1p (Benard et al., 1999). If Tef1p is a *bona fide* Rho1p effector, we would expect to see preferential binding of Tef1p to the GTP-bound state of Rho1p. To assess this we performed a chemical nucleotide exchange reaction in the absence or presence of GDP or GTP γ S on glutathione resin-bound GST-Rho1p and on Tef1p-GFP from yeast lysate. GTP γ S is a non-hydrolysable analogue of GTP which locks Rho1p in an “active” state. This allowed us to

predetermine the nucleotide-bound state of Rho1p and Tef1p for interaction studies. We observed that Tef1p showed preferential binding to the GDP-bound state of GST-Rho1p (**Fig. 5A**). We also observe that in all cases the GDP-bound state of Tef1p showed preferential binding to Rho1p (**Fig. 5B**). This contradicts our hypothesis that Tef1p is an effector molecule of Rho1p since we expected to see Tef1p binding to the GTP γ S-bound state of Rho1p if Tef1p were a Rho1p effector. The lower affinity of GTP γ S-bound Tef1p for Rho1p makes logical sense since Tef1p-GTP is important for protein synthesis and so may be functionally shuttled over to that role by Tef1p GEFs (Pittman et al., 2009).

3.4 Analysis of Tef1p sub-domains for Rho1p interaction

Tef1p is comprised of three distinct domains. Domain 1 (amino acids 1-219), which contains the GTP-binding domain and a calmodulin binding domain, domain 2 (a. a. 220-319) which contains the aminoacyl tRNA-binding domain as well as a calmodulin binding domain, and domain 3 (a. a. 320-436) which contains another calmodulin binding domain and the actin binding domain (**Fig. 6A**) (Morita et al., 2008). The crystal structure has been solved in complex with Tef5p, the GEF for Tef1p (**Fig. 6A**). Tef5p interacts with both domain 1 and domain 2 (Andersen et al., 2000). Here, we attempted to determine which Tef1p sub-domain(s) is required for binding to Rho1p. GFP-Tef1p full length (FL) and sub-domain constructs were cloned and expressed in yeast. Yeast lysates were incubated with both MBP-Rho1p

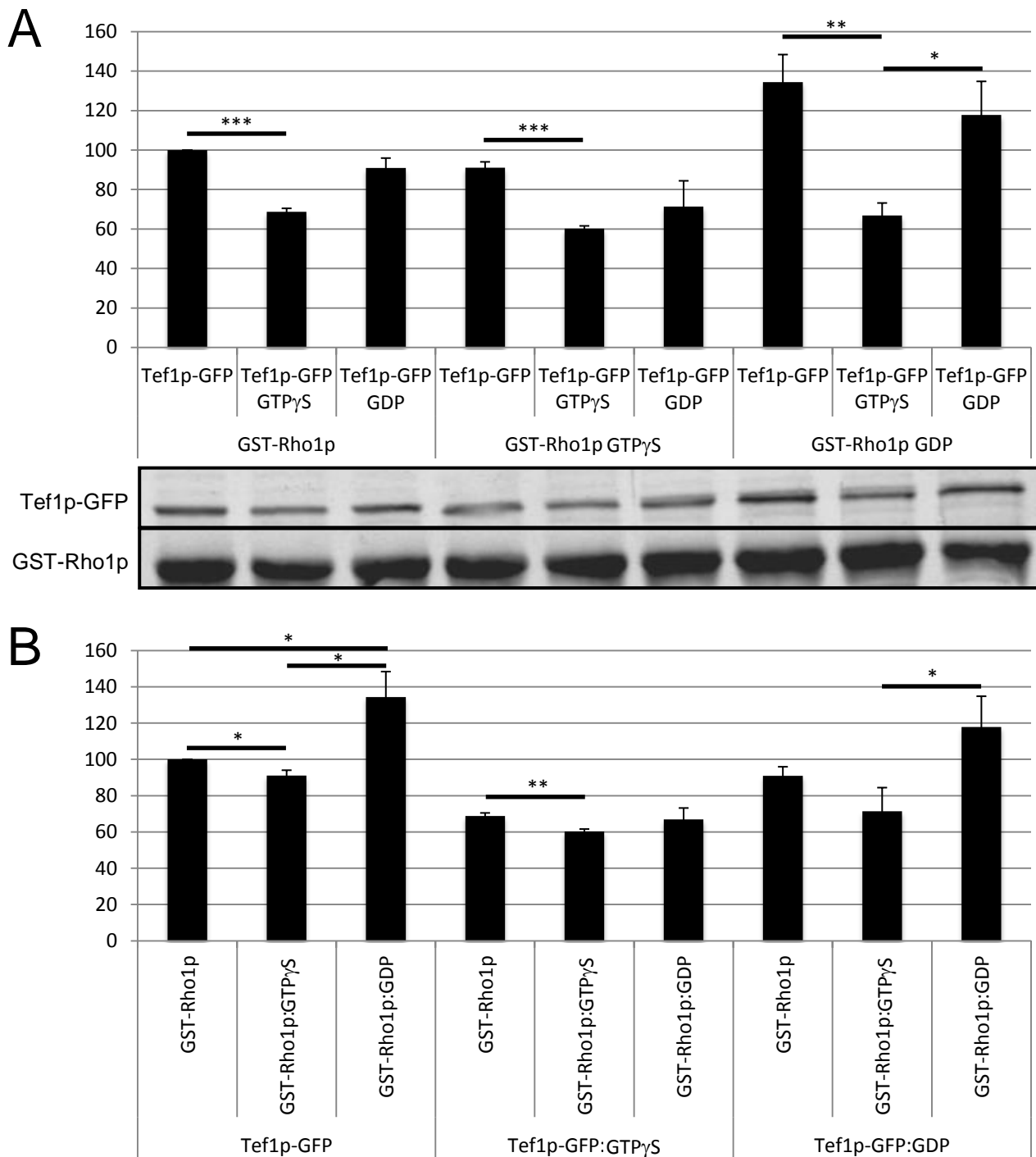


Figure 5. Tef1p:GDP and Rho1p:GDP are the preferred nucleotide states for interaction. Chemical nucleotide exchange was performed on Tef1p-GFP from yeast lysate before incubation with chemical nucleotide exchanged resin-bound GST-Rho1p. Bound fractions were subjected to SDS-PAGE and analyzed by immunoblot and densitometry. (A) Comparison of Tef1p-GFP nucleotide-bound species binding to immobilized GST-Rho1p, with a representative immunoblot shown in the lower panel. (B) Re-arrangement of data from Fig. 4A to illustrate specificity of GST-Rho1p nucleotide-bound species to Tef1p-GFP nucleotide-bound species. Binding experiments were repeated at least 3 times and levels were normalized to GST-Rho1p/Tef1p-GFP without nucleotide exchange for each experiment. The relative differences in binding were compared for significance by Student's *t*-test (*, $P < 0.05$; **, $P < 0.01$; ***, $P < 0.001$; n.s., $P > 0.05$, not shown).

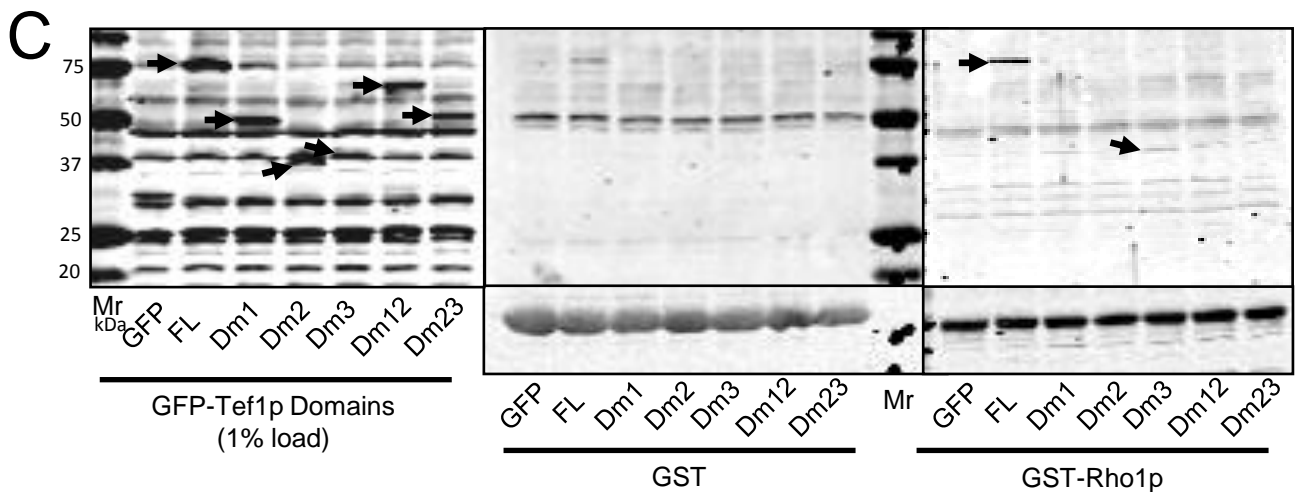
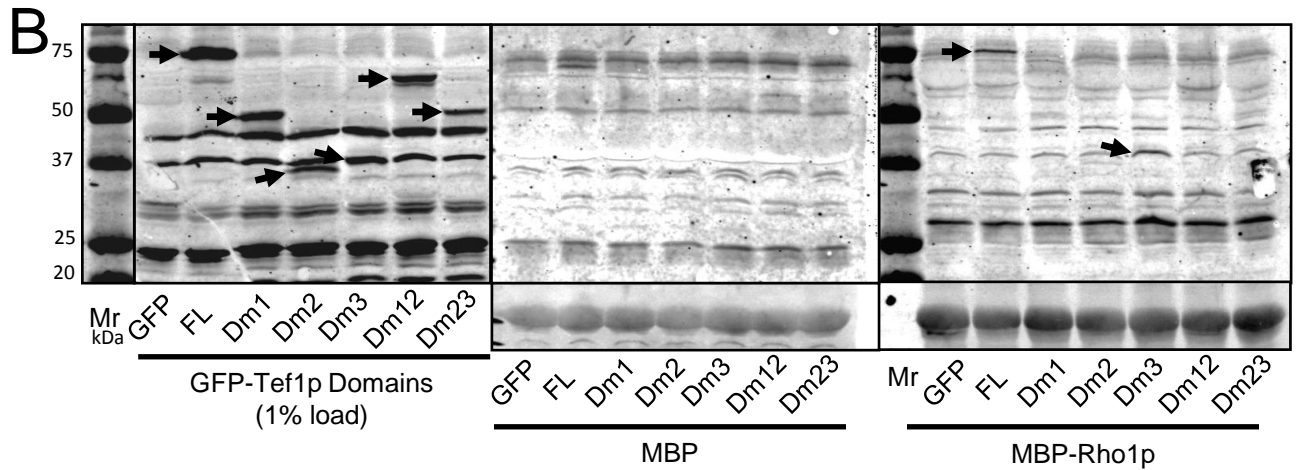
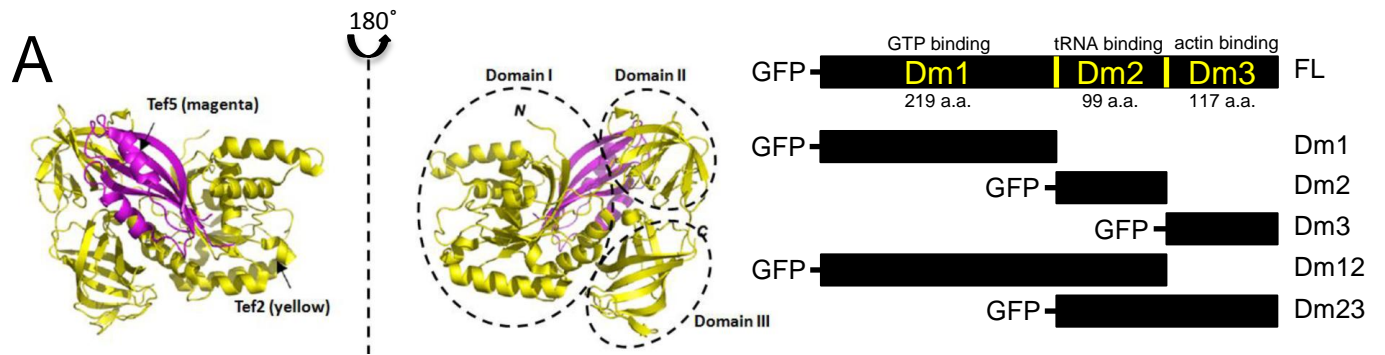
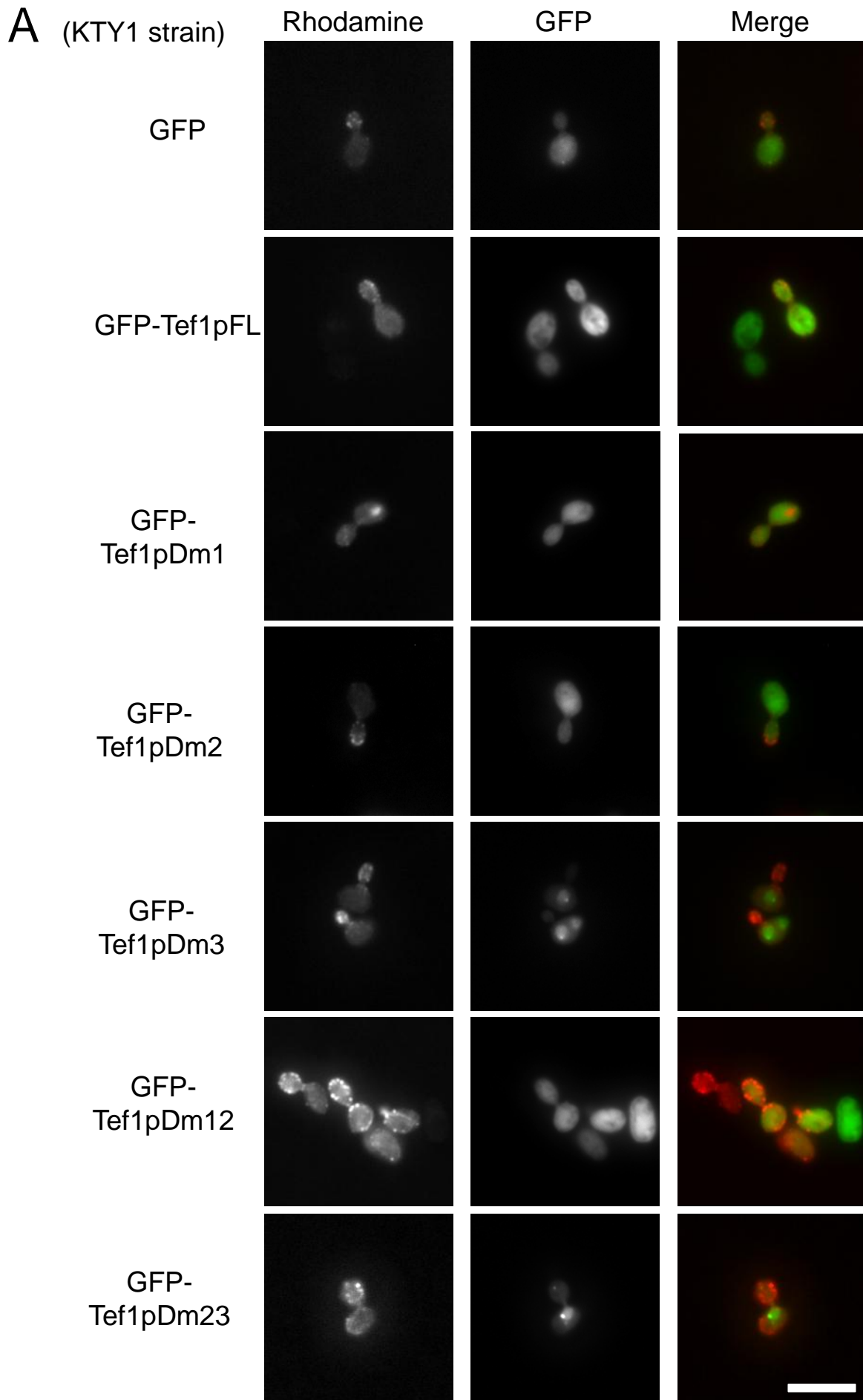


Figure 6. Rho1p-binding domains of Tef1p. (A) Tef1p three dimensional structure in association with Tef5p, highlighting sub-domains (Soares et al., 2009). (B and C) 10 mg of yeast lysate from KTY1 strains expressing GFP or GFP-Tef1p (FL) or GFP-Tef1p domains were incubated with amylose resin-bound MBP or MBP-Rho1p (B) and glutathione resin-bound GST or GST-Rho1p (C). Bound fractions were subjected to SDS-PAGE and analyzed by immunoblot.

(Fig. 6B) and GST-Rho1p **(Fig. 6C)**. In both cases GFP-Tef1p FL was the only construct to show significant association with MBP-Rho1p or GST-Rho1p. We also observed some background binding of GFP-Tef1p FL when incubated with MBP and GST; however, this was consistently significantly less than in Rho1p pull-downs. Our anti-GFP immunoblots showed numerous background bands regardless of the source of antibody. This was especially true around 40 kDa which correlates with our GFP-Tef1p domain 3 (Dm3) construct, which does appear to show slight binding to Rho1p. These data suggest that the full-length Tef1p is necessary for optimal binding and that the Rho1p-binding regions of Tef1p may span 2 or more sub-domains, as they do in the case of Tef5p.

3.5 GFP-Tef1p sub-domain localization and effects on the actin cytoskeleton.

Previously, overexpression of Tef1p has been shown to cause disorganization of the actin cytoskeleton leading to cell growth defects (Munshi et al., 2001). This led us to an examination of the effects of expressing GFP-Tef1p sub-domains on the actin cytoskeleton and whether a domain showed any distinct localization. We performed this experiment under conditions of either endogenous Rho1p levels or when overexpressed, in the form of 3xHA-Rho1p, to see if this had any effect as well **(Fig. 7, panels A vs B)**. GFP-Tef1p FL was ubiquitously localized throughout the cell, similar to GFP alone, this was also observed in the case of GFP-Tef1p Dm1, Dm2, and



B (HA-RHO1 strain)

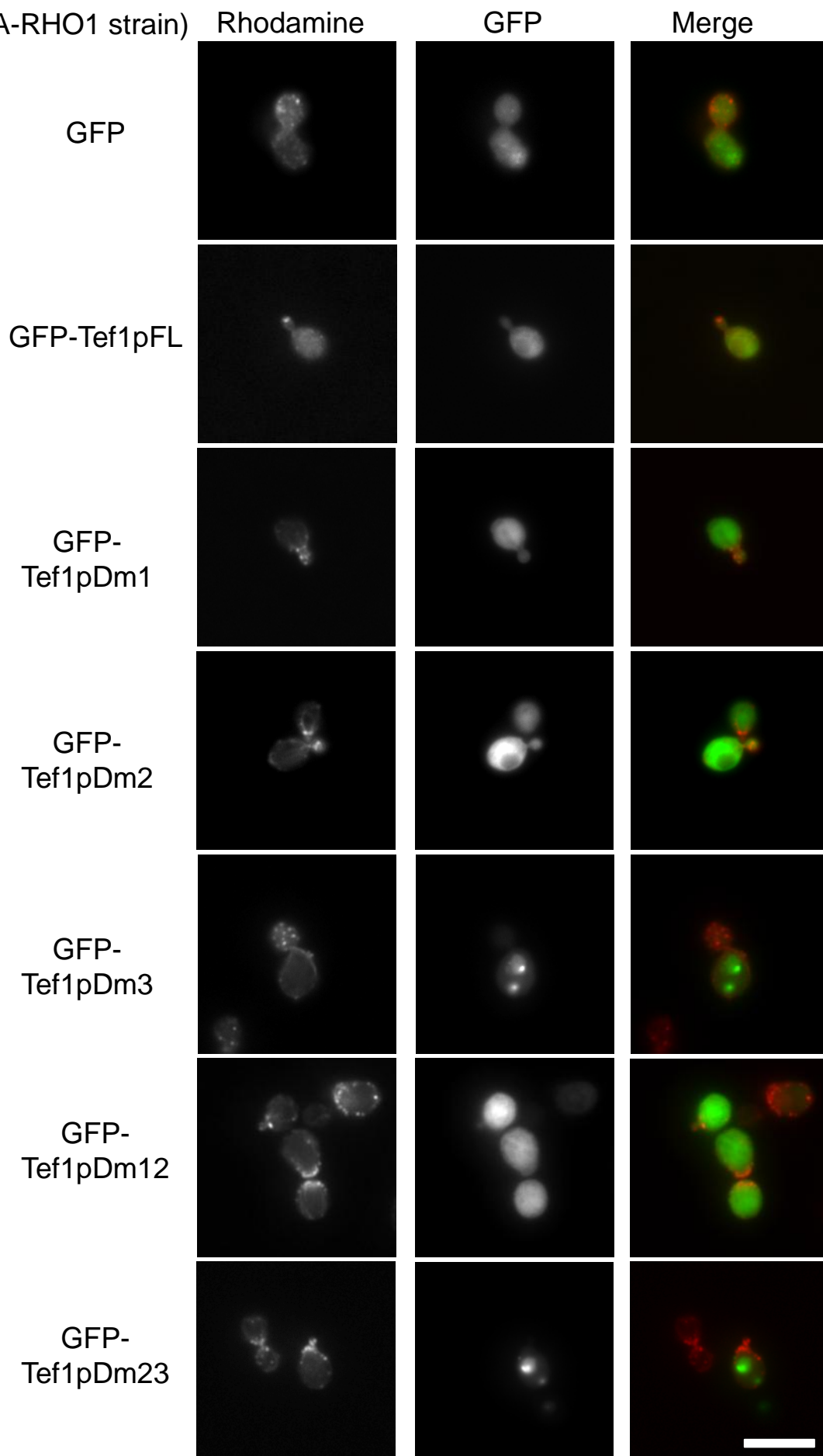
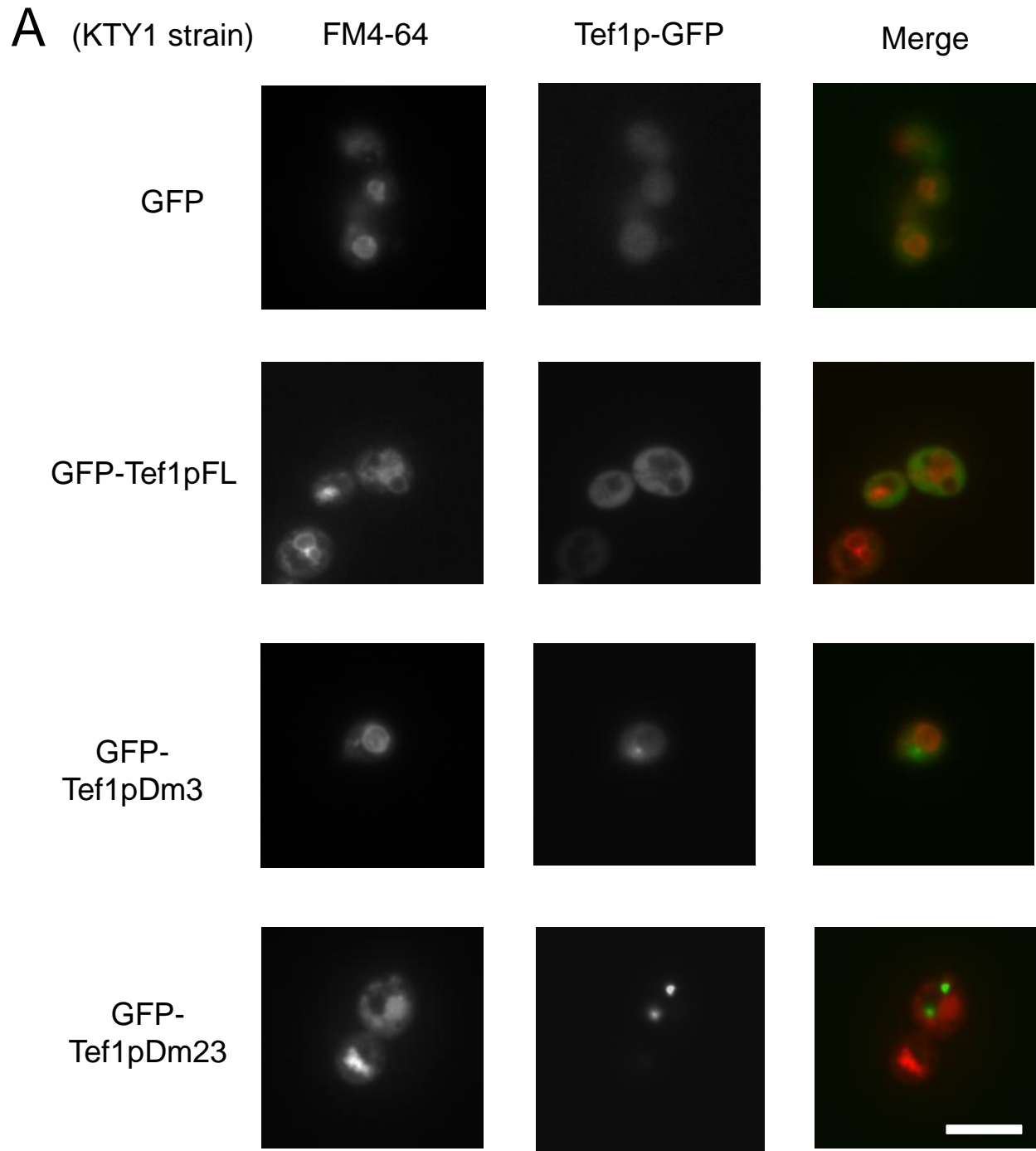


Figure 7. Actin cytoskeleton morphology and GFP-Tef1p domain localization. (A and B) Images of cells from the yeast strain KTY1 (A) or HA-RHO1 (B) expressing GFP, GFP-Tef1p, or GFP-Tef1p sub-domain constructs were grown in expression medium. Cells were fixed and stained with rhodamine phalloidin and analyzed by fluorescence microscopy. The yeast strain HA-RHO1 is KTY1 that overexpresses 3xHA-Rho1p from the P_{GAL} promoter. Cells were imaged while in log phase at 100X magnification, 1.4 NA using a Zeiss Axio wide-field microscope and a Hamamatsu CoolSNAP HQ camera. Images were taken with ImageJ and processed with Adobe Photoshop. Confirmation of expression by SDS-PAGE and immunoblot analysis is provided in Appendix A. Bar = 5 μm



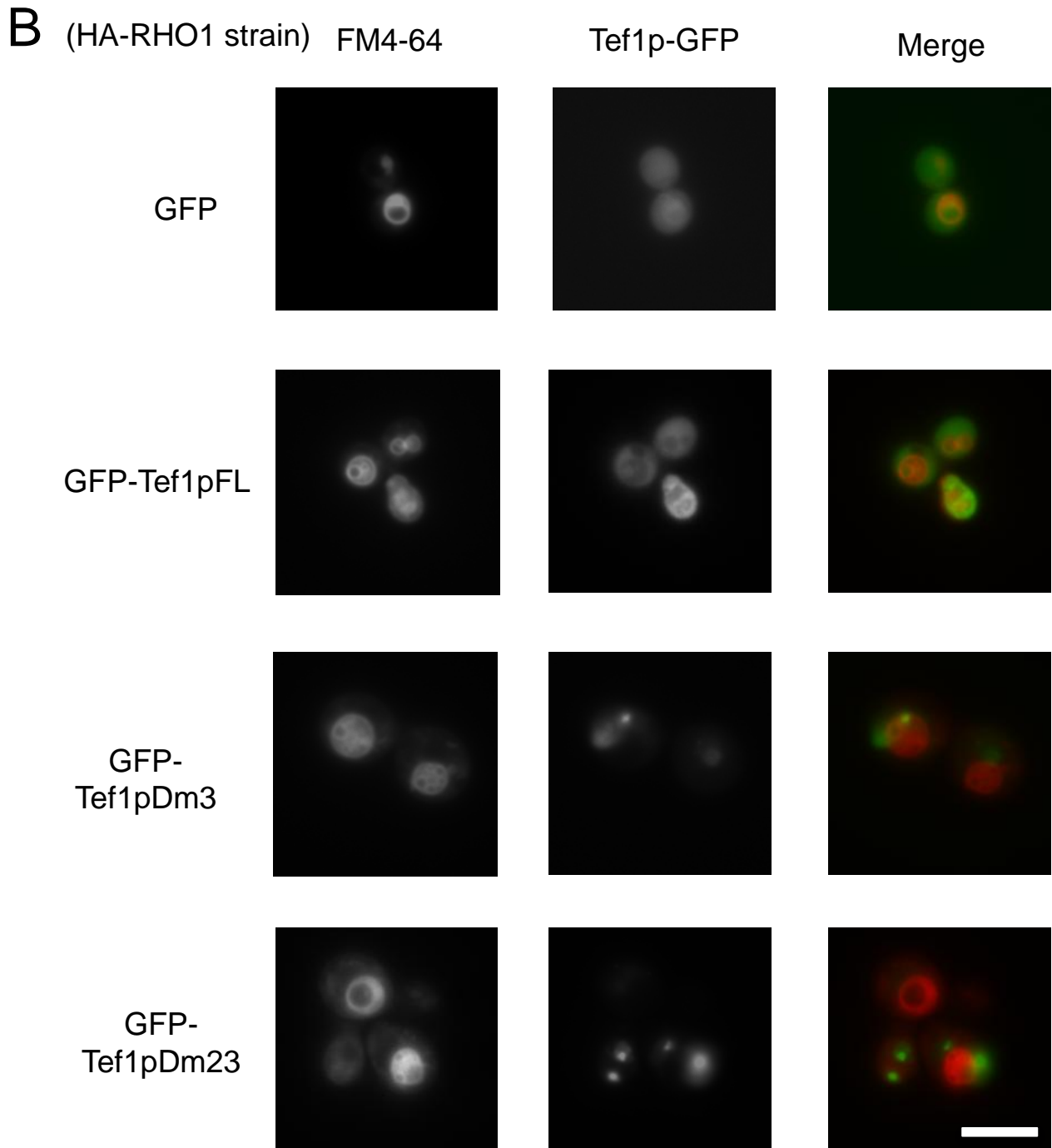


Figure 8. Vacuole morphology and GFP-Tef1p domain localizations. (A and B) Images of cells from the yeast strain KTY1 (A) or HA-RHO1 (B) expressing GFP, GFP-Tef1p, or GFP-Tef1p sub-domains Dm3 and Dm23 were grown in expression medium. Cells were fixed and stained with FM4-64 to label vacuoles and analyzed by fluorescence microscopy. The yeast strain HA-RHO1 is KTY1 that overexpresses 3xHA-Rho1p from the P_{GAL} promoter. Cells were imaged while in log phase at 100X magnification, 1.4 NA using a Zeiss Axio wide-field microscope and a Hamamatsu CoolSNAP HQ camera. Images were taken with ImageJ and processed with Adobe Photoshop. Confirmation of expression by SDS-PAGE and immunoblot analysis is provided in Appendix A. Bar = 5 μ m

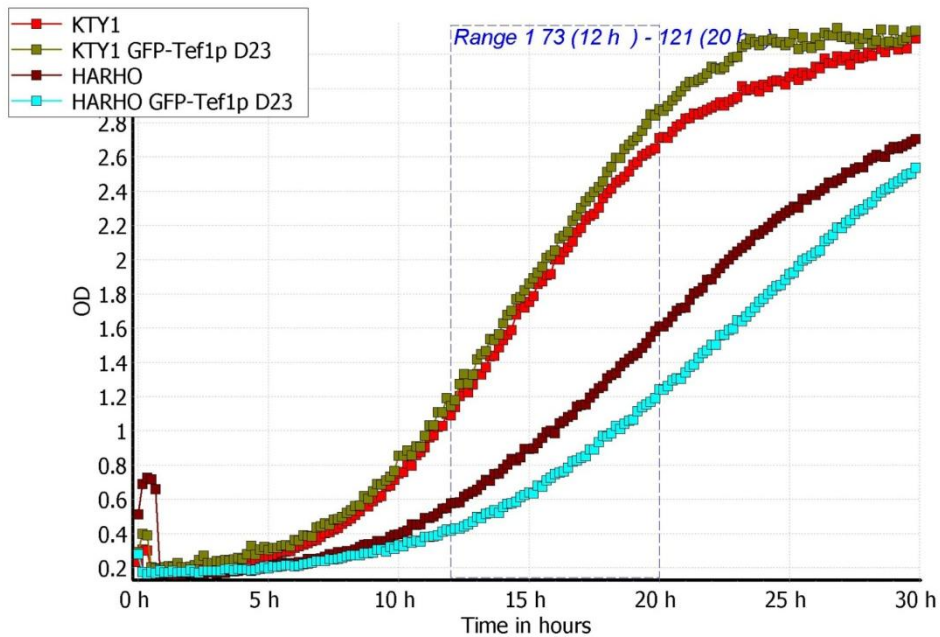
Dm12 constructs in both strains (**Fig. 7, A and B**). Interestingly, we found that GFP-Tef1p Dm3 or GFP-Tef1p Dm23 formed puncta that localized to the vacuole membrane (**Fig. 8**) with an appearance similar to what we observe with vacuoles isolated from Tef1p-GFP expressing cells (*see Fig. 3B*). This suggests that domain 3 may be responsible for localization to the vacuole membrane and that domain 1 may act as a regulator of localization since the constructs that lack domain 1 (GFP-Tef1p Dm23 and GFP-Tef1p Dm3) showed similar localization (**Fig. 7 and 8**). When filamentous actin is stained using rhodamine-phalloidin, we did not observe any striking cytoskeletal defects as actin patch localization to the bud tip looked normal (**Fig. 7 all panels**). It is possible that by using GFP-tagged constructs that we are perturbing the ability of Tef1p to bind and bundle actin, as previous studies have shown that the packing order of Tef1p with actin is fairly tight and likely excludes the binding of other proteins (Owen et al., 1992).

We wished to observe what effects the GFP-Tef1p domain constructs might have on growth rates and whether or not those effects would be abrogated by the overexpression of 3xHA-Rho1p. Preliminary results suggest that the expression of the GFP-Tef1p domain constructs had little effect on the growth rates of strains with endogenous levels of Rho1p (KTY1 strain) (**Appendix B**). When 3xHA-Rho1p was overexpressed, we observed a general inhibition of growth from a doubling time of 2.89 h for KTY1, to 4.51 h for the 3xHA-Rho1p expressing strain. Expression of GFP-Tef1p sub-domain constructs appear to further inhibit the growth rates in the 3xHA-

Rho1p overexpression strain, but this needs to be further investigated (**Fig. 9**). This was surprising since we thought that if there was a GFP-Tef1p sub-domain construct that would inhibit the growth rates, by potentially perturbing the normal protein translational machinery or causing aberrant cytoskeletal organization, this would be recovered by overexpression of 3xHA-Rho1p if the perturbation was due to dysfunction of the Tef1p-Rho1p interaction. However, it appears that overexpression of 3xHA-Rho1p on its own is causing a significant growth defect that may mask the effects of the GFP-Tef1p constructs.

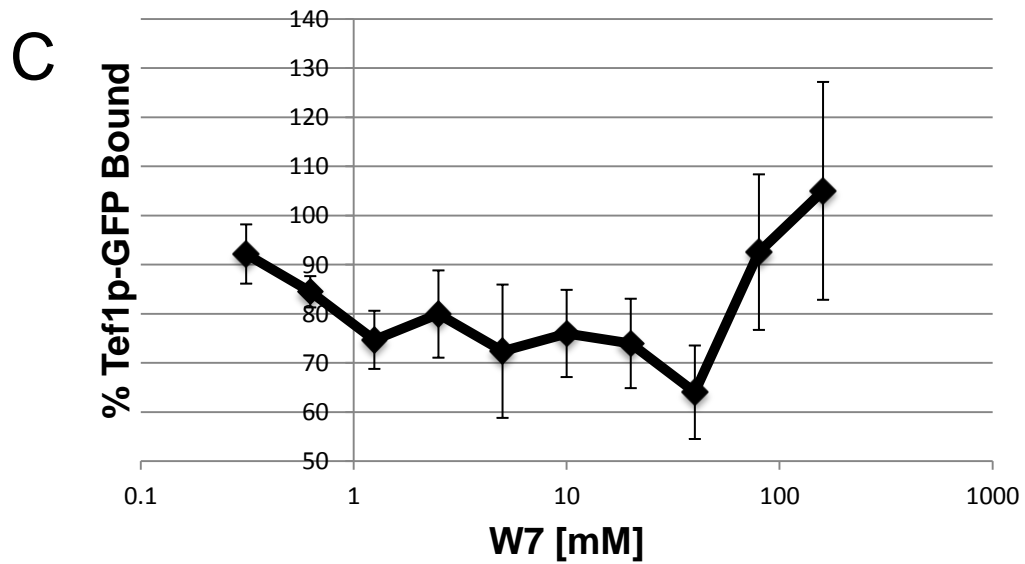
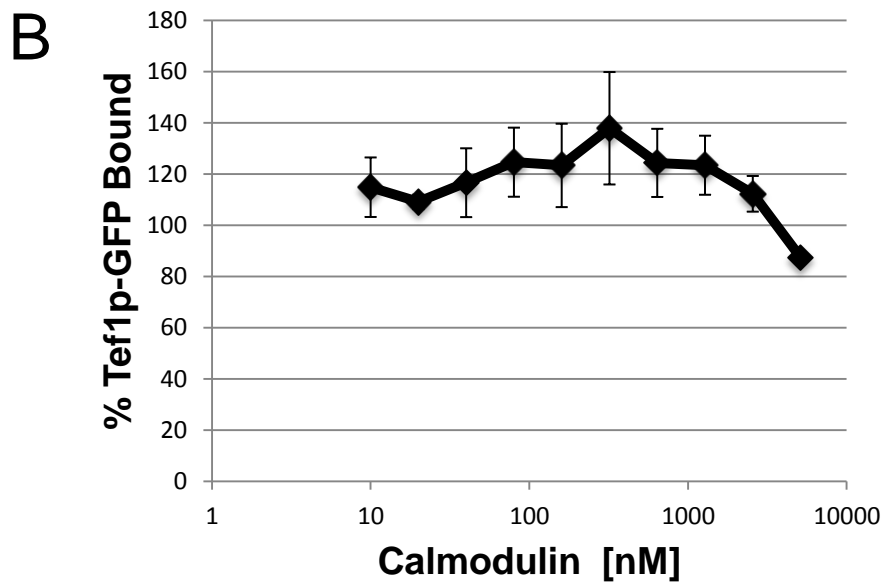
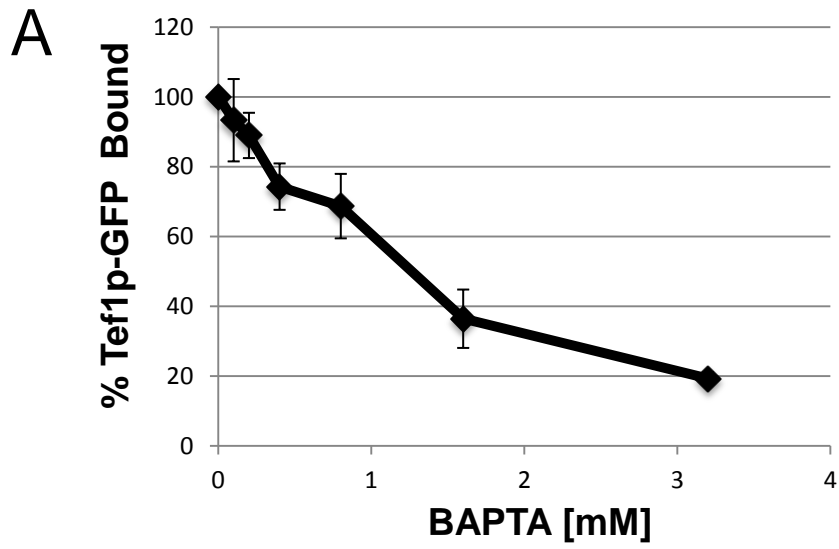
3.6 Modulation of Tef1p::Rho1p interaction.

Previously, a connection between calcium and the actin bundling activity of *Tetrahymena* eEF1A had been shown where concentrations greater than 1 μ M calcium were found to lead to increased binding of calmodulin, a calcium signaling molecule, and inhibition of actin bundling properties (Morita et al., 2008). To investigate a potential link between calcium signaling and the Tef1p:Rho1p interaction, we performed affinity purification of Tef1p-GFP with glutathione resin-bound GST-Rho1p in the presence of the calcium specific chelator BAPTA (**Fig. 10A**). We found that BAPTA inhibited Tef1p:Rho1p binding in a dose dependent manner up to 80% at 3.2 mM BAPTA. This indicates that calcium is necessary for Tef1p binding to Rho1p. Next, we investigated the role of calmodulin in the Tef1p::Rho1p interaction by affinity pull-down. This affinity interaction was



Construct	Doubling Time, DT (h)		Δ DT (construct vs none)	
	KTY1	HA-RHO1	KTY1	HA-RHO1
none	2.89	4.51		
GFP	2.77	4.78	-0.12	0.27
GFP-Tef1p FL	2.81	4.38	-0.08	-0.13
GFP-Tef1p Dm1	2.72	5.01	-0.17	0.50
GFP-Tef1p Dm2	2.86	4.26	-0.03	-0.25
GFP-Tef1p Dm3	2.99	4.90	0.10	0.39
GFP-Tef1p Dm12	2.96	4.93	0.07	0.42
GFP-Tef1p Dm23	2.80	5.28	-0.09	0.77

Figure 9. Effect of GFP-Tef1p full-length and sub-domain expression on growth rates of wild-type and HA-RHO1 overexpressing yeast. Wild-type yeast (KTY1) and yeast over-expressing 3xHA-Rho1p (HA-RHO1) were examined for changes in growth rates when transformed with constructs expressing GFP-Tef1p full-length and sub-domains as indicated in Figure 5A. Strains were incubated at 30°C in a CLARIOstar plate reader with agitation and optical density was measured at 600 nm over 30 h at 10 min intervals. Doubling time was determined by taking the maximum slope over a 12 time point range between 12 h and 20 h. Sample curves for GFP-Tef1p full-length and Dm23 are shown. All growth curves are available in Appendix B.



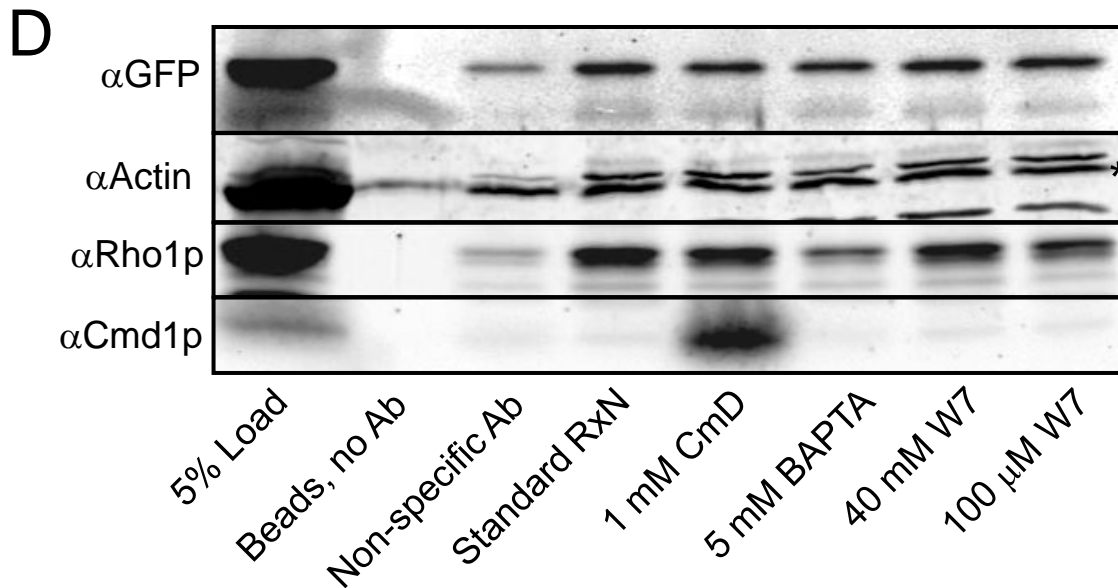


Figure 10. Effects of calcium/calmodulin on Tef1p::Rho1p interaction. (A) Analysis of the binding of Tef1p and Rho1p. 0.5 mg of lysate from Tef1p-GFP expressing yeast was incubated with glutathione resin-bound GST-Rho1p (10 μ l packed resin) in the presence of increasing concentrations of BAPTA, a calcium-specific chelator. (B) A binding experiment was performed as described in A, except calmodulin, a calcium-binding signaling molecule, was added in increasing concentrations. (C) A Tef1p::Rho1p binding experiment was performed as described in A, except in the presence of increasing concentrations of W7, a calmodulin-specific inhibitor. Graphs are on varying scales to suit concentration ranges and responses. (D) Immunoprecipitation of GFP-Tef1p with rabbit anti-GFP coated protein A beads. Rho1p shows specific co-immunoprecipitation with GFP-Tef1p. Addition of BAPTA or the calmodulin inhibitor, W7, reduces the levels of Rho1p association while the addition of exogenous calmodulin (CmD) has no effect on the Rho1p levels. *, non-specific band

performed in the presence of recombinant yeast calmodulin over a concentration range from 0 - 5.12 μM (**Fig. 10B**). While it appeared that there was an increase in binding over the range of 0 - 320nM calmodulin, no statistical difference was observed when performing a Student's *t*-test with a p-value of < 0.05 . Inhibition was observed at extremely high concentrations of calmodulin, but this could be due to non-specific effects. We next decided to perform an assay where calmodulin activity was inhibited using the drug W7. W7 has been shown to bind calcium-bound calmodulin and inhibit binding to downstream target proteins and membrane fusion (Osawa et al., 1998, Peters and Mayer, 1998). We performed affinity pull-down assays in the presence of increasing concentrations of W7 (**Fig. 10C**). We observed an inhibition of binding of up to 36% at 40 μM W7 that was shown to be statistically significant when a Student's *t*-test was performed with a p-value of < 0.01 . At very high W7 concentrations we observed the recovery of GFP-Tef1p binding to GST-Rho1p. To support the findings of these experiments we performed co-immunoprecipitation against Tef1p-GFP and blotted for endogenous Rho1p binding. This experiment showed similar results as those in Figures 10A-C, with calmodulin having little effect, BAPTA decreasing binding and W7 decreasing binding (**Fig. 10D**). This provides evidence that calcium-calmodulin binding to Tef1p is playing a role in the affinity of Tef1p with Rho1p but the precise involvement will need to be further elucidated.

Tef5p, the GEF for Tef1p, has previously been shown to disrupt the actin bundling properties of Tef1p where it is thought that it is able to shift

the function of Tef1p from an actin bundling protein into the role of aminoacyl-tRNA transferase in protein translation (Pittman et al., 2009). We decided to investigate the effects that Tef5p might have on the Tef1p::Rho1p interaction (**Fig. 11**). We observed that Tef5p was able to significantly inhibit the association of GFP-Tef1p to GST-Rho1p in a dose dependent manner, by as much as 89% at 3.2 μ M. This suggests that Tef5p and Rho1p competitively bind the same region of Tef1p. Since pulldowns were performed at 4°C, this would minimize any potential GEF activity that might be taking place in the reaction.

Narciclasine, a small molecule drug isolated from plants of the Amaryllidaceae family, had been identified as inducing RhoA (mammalian Rho1p) activation and stress fiber formation in glioblastoma cells (Lefranc et al. 2009) but direct binding of narciclasine to RhoA had not been investigated. Narciclasine had then been shown to specifically bind to Tef1p and impair Tef1p actin bundling as well as affect protein initiation and translation (Van Goietsenoven et al. 2010). While both of these characteristics were identified, there had never been any mention of functional linkage between the effects of narciclasine on Tef1p and Rho1p activation. This was the first evidence that perhaps Tef1p lies upstream of Rho1p and is involved in the activation of Rho1p. To test this, we wanted to see if narciclasine had any effect on the Tef1p::Rho1p interaction in the

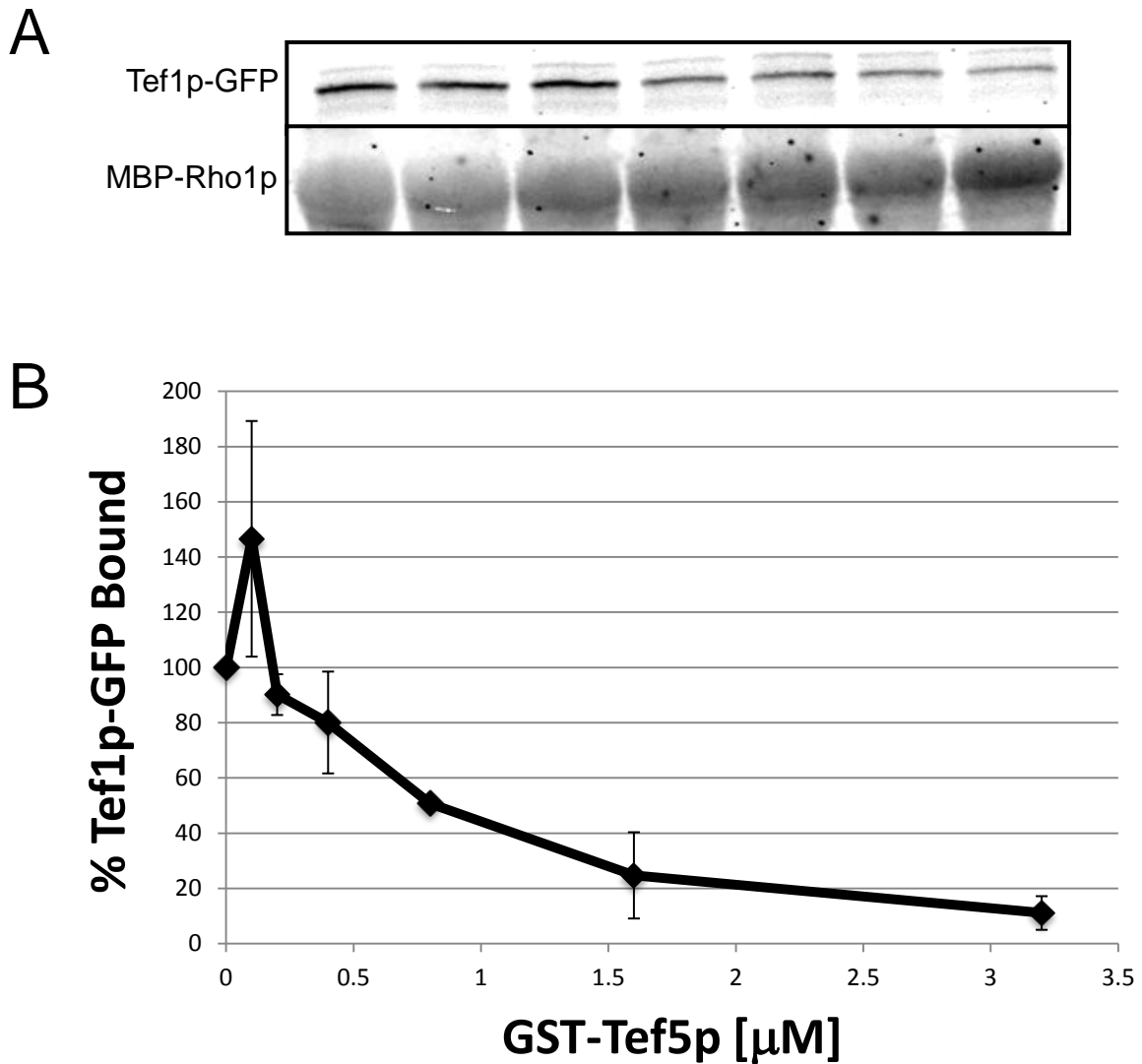


Figure 11. Effects of Tef5p, the guanine nucleotide exchange factor (GEF) of Tef1p, on Tef1p::Rho1p interaction. Lysate isolated from Tef1p-GFP expressing yeast was incubated with amylose resin-bound MBP-Rho1p in the presence of increasing concentrations of purified GST-Tef5p. (A) Immunoblot of typical reaction. (B) Bound fractions were subjected to SDS-PAGE and analyzed by immunoblot and quantified by densitometry.

presence of calcium. Here we found that narciclasine had no significant effect on the Tef1p:Rho1p interaction in the presence of calcium until concentrations of 10 μ M (higher ranges were not tested) where an inhibition of 40% was observed (**Fig. 12**). This contradicted our hypothesis as we would expect to see increased association if narciclasine was working through Tef1p in the Rho1p activation pathway. Further investigation is needed to identify whether narciclasine is a ligand of yeast Tef1p.

3.7 Tef1p effect on vacuole membrane fusion

Considering that our original hypothesis was to that Tef1p was a Rho1p effector molecule involved in membrane fusion, we next performed membrane fusion assays using yeast vacuoles in the presence of excess MBP-Tef1p, MBP-Tef5p, narciclasine and W7 (**Fig. 13**). When we performed fusion experiments in the presence of MBP-Tef1p and MBP-Tef5p, we found relatively little effect on membrane fusion when compared to the addition of MBP alone (**Fig.13A**). When membrane fusion assays were performed in the presence of increasing concentrations of narciclasine, we observed an inhibitory effect from 1-100 nM that was abrogated by addition of MBP-Tef1p suggesting that the inhibitory effect on fusion is specifically due to the binding of narciclasine to Tef1p (**Fig. 13B**). We also found that when we added the calmodulin inhibitor W7, there was a significant inhibition from 10 nM – 10 μ M (**Fig. 13C**). This would be expected as calcium-calmodulin

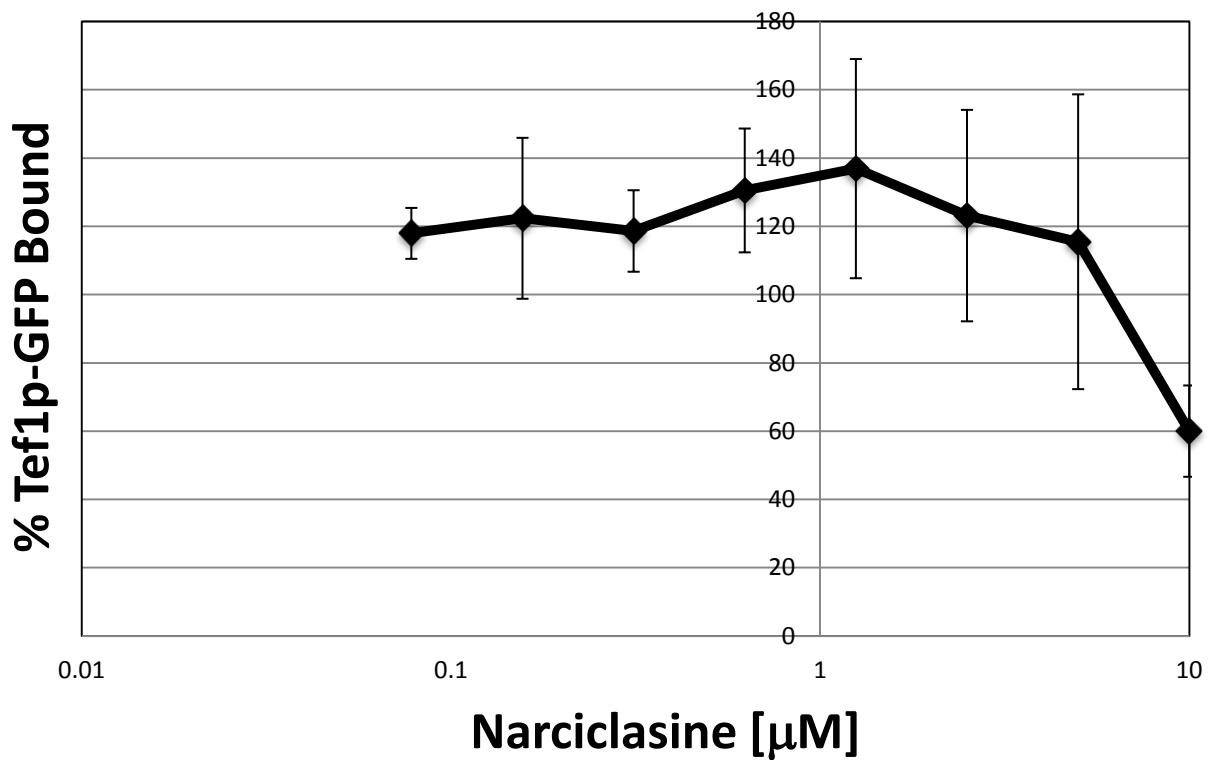
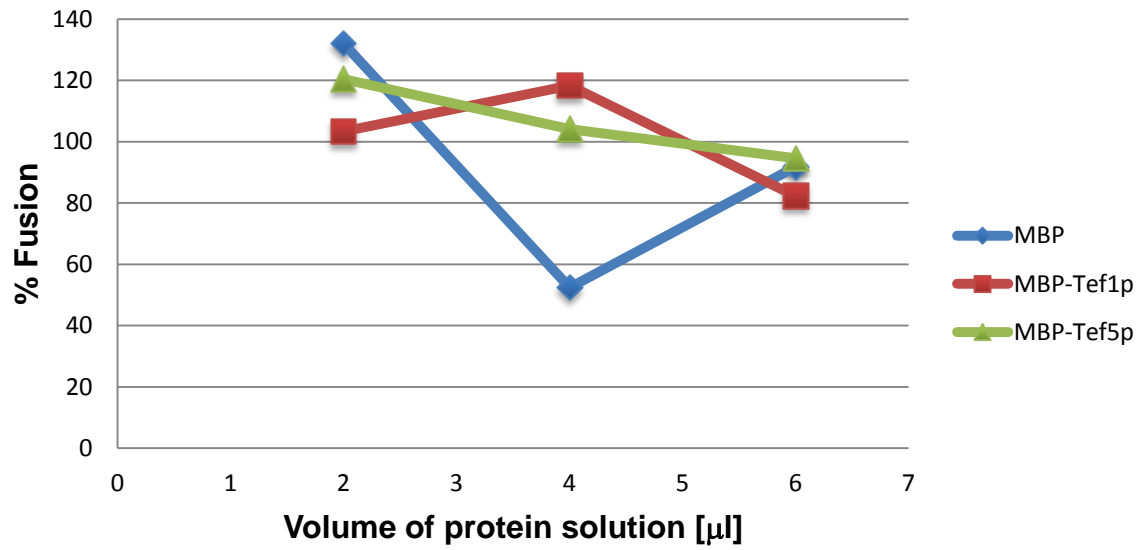
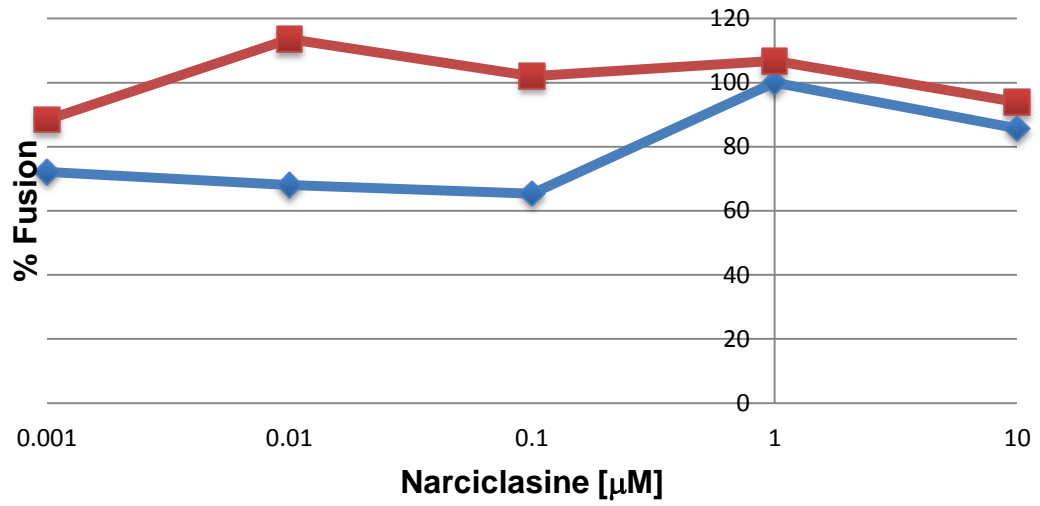


Figure 12. Effect of narciclasine, a GTPase targeting drug, on Tef1p:Rho1p interaction. Lysate isolated from Tef1p-GFP expressing yeast was incubated with amylose resin-bound MBP-Rho1p in the presence of 2 mM CaCl₂ and increasing concentrations narciclasine. Bound fractions were subjected to SDS-PAGE and analyzed by immunoblot and quantified by densitometry.

A



B



C

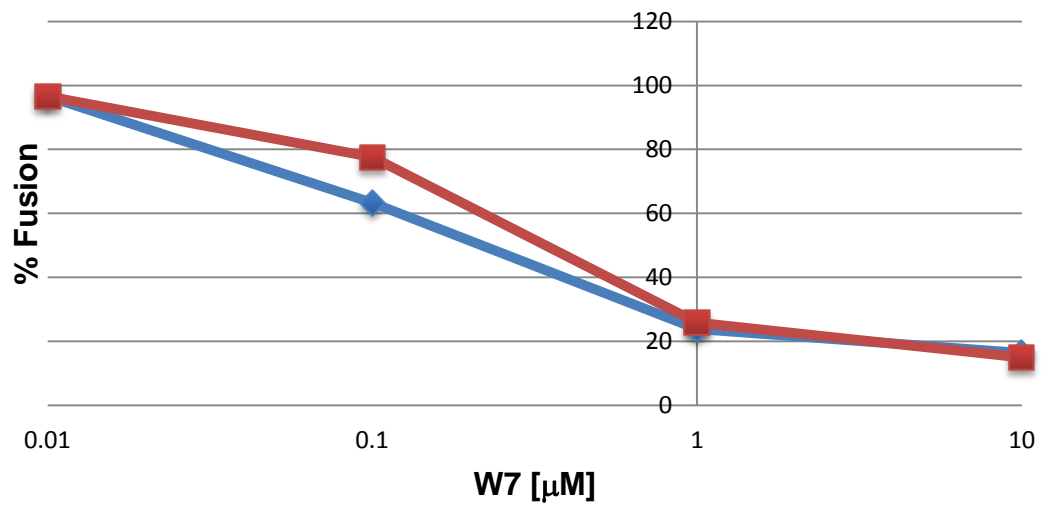


Figure 13. Effects of Tef1p, Tef5p, narciclasine, and W7 on membrane fusion. Yeast vacuole fusion experiments were performed in the presence of increasing volumes of MBP, MBP-Tef1p, or MBP-Tef5p with respective stock concentrations of 4.1, 2.7, and 1.75 mg/ml (A), increasing concentrations of narciclasine with a 6 μ l of MBP (blue) or MBP-Tef1p (red) (B), or increasing concentrations of W7 with a 6 μ l of MBP (blue) or MBP-Tef1p (red) (C).

activity has previously been shown to be involved in membrane fusion
(Peters and Mayer, 1998)

CHAPTER 4

DISCUSSION

4.1 Tef1p is not a downstream effector molecule of Rho1p

In *S. cerevisiae*, two Rho-family GTPases have been identified as being essential in the late stages of vacuole fusion, Cdc42p and Rho1p (Eitzen et al. 2001). Activation of the two Rho GTPases occurs sequentially with an initial activation of Cdc42p followed by activation of Rho1p (Logan et al., 2010). An essential actin polymerization step in membrane fusion had been shown to be associated with Cdc42p activation (Isgandarova et al., 2007), while the downstream effects of Rho1p had not yet been elucidated.

Upon initial identification of Tef1p as a Rho1p binding protein on vacuole membranes (**Fig. 2A**), our hypothesis was that Tef1p was a downstream effector molecule of Rho1p. Therefore, upon Rho1p activation, the actin bundling activity of Tef1p would be induced. The specificity for binding of downstream effectors of Rho1p to GTP:Rho1p has been used for assaying Rho1p activation (Ren et al., 1999). In our case we used chemical nucleotide exchange to lock Rho1p in both the “on” and “off” conformation and then probe for Tef1p. Our hypothesis was if Tef1p is an effector molecule of Rho1p, then we would expect Tef1p to be preferentially bound to GTP:Rho1p over GDP:Rho1p. However this was not the case and the preferred binding state was GDP:Rho1p (**Fig. 5A**). Considering that Tef1p is itself a GTPase, we also prepared GFP-Tef1p in various nucleotide states which we thought may offer some further insight into the interaction. We found that the preferred binding state of Tef1p to Rho1p was also GDP:Tef1p (**Fig. 5B**). While previous studies have shown that the actin bundling activity

of Tef1p is not regulated by the nucleotide-bound state (Edmonds et al., 1998), this suggests that perhaps the nucleotide state of Tef1p may modulate the function of Tef1p between actin dynamics, where the GDP-bound form functions, and protein translation, where the GTP-bound form is necessary for function. Overall, this suggests that Tef1p is not an effector molecule of Rho1p but the interaction may have some other significance.

4.2 Rho1p-interacting domain of Tef1p

Attempts to purify GST-Tef1p domain fusion proteins from *E. coli* were met with little success. We therefore, attempted to express GFP-Tef1p sub-domains in yeast and to attempt to identify the Rho1p-interacting domain of Tef1p. This would provide valuable information on the interaction and guide us to a potential specific binding site that we would be able to use for site-directed mutagenesis to further elucidate the role of the Tef1p:Rho1p interaction. While we saw an interaction between the full length GFP-Tef1p and GST-Rho1p or MBP-Tef1p, and a slight interaction with GFP-Tef1p Dm3 (**Fig. 6**), the interaction did not appear as strong as when we used C-terminally tagged Tef1p (see representative immunoblot in **Fig. 5** where 2 mg total Tef1p-GFP lysate was added). It is possible that N-terminally tagging Tef1p interfered with the Tef1p-Rho1p interaction. The difficulties that we had in purification could be that domain 3 of Tef1p consists of β -barrel structures that could potentially aggregate (Maitra and Nowick, 2000). With regards to the microscopy and growth data (**Figs. 7 - 9**), it is possible that the

size of the GFP-tag on the proteins could be sterically interfering with the binding of the Tef1p domains with some of their normal binding partners (e.g. the ribosome or actin), thus not offering much insight into the actions of these domains *in vivo*. A potential solution to this problem might be to attempt to use smaller tags such as His₆-tags.

4.3 Involvement of Calcium/Calmodulin on the Tef1p:Rho1p interaction

After we determined that Tef1p was not an effector molecule of Rho1p, we investigated potential modulators of the Tef1p:Rho1p interaction to assist in elucidating the functional role of the interaction. As shown by Morita et al. (2008), calcium signaling through calmodulin is able to regulate the actin bundling properties of Tef1p. Additionally, calcium/calmodulin has previously been shown to be involved in the regulation of Rac1 and Cdc42 in platelet cells where it bound to both Rac1 and Cdc42, but had opposing effects on each; it increased activation of Rac1 and decreased activation of Cdc42 (Elsaraj and Bhullar, 2008). In the same study, they used W7 as a calcium/calmodulin antagonist and found that W7 was able to inhibit activation of Rac1 while enhancing activation of Cdc42. Thus we decided to see what effect calcium and calmodulin would have on the Tef1p:Rho1p interaction (**Fig. 10**). BAPTA, a calcium specific chelator, was able to efficiently inhibit the association of Tef1p-GFP with GST-Rho1p, suggesting that the association is calcium dependent (**Fig. 10A**). The next question was then to determine if the calcium effect was due to association of Tef1p with

calmodulin. We used purified calmodulin as well as W7, a calmodulin inhibitor, to determine what, if any, role calmodulin might be playing in the interaction. We found that calmodulin was able to increase binding of Tef1p-GFP to GST-Rho1p by up to 40% (**Fig. 10B**) and W7 had an inhibitory effect up to 36% at 40 μ M on the binding of GFP-Tef1p to GST-Rho1p (**Fig. 10C**). Interestingly, when we perform co-immunoprecipitation for Tef1p-GFP, we see only slight association of calmodulin with Tef1p-GFP. We were able to further saturate GFP-Tef1p with calmodulin, but with little effect on Rho1p association (**Fig. 10D**). This suggests that the interaction may occur at low levels of calmodulin associated with Tef1p.

4.4 Potential roles for Tef1p in Rho1p activation and membrane fusion

Previous studies have shown that the Rho family GTPases Cdc42p and Rho1p are activated sequentially after tethering. Cdc42p activation occurs early followed by calcium flux and Rho1p activation (Logan et al., 2010; Eitzen et al., 2000). Recently, the proteins Ack1p and Rgl1p have been identified as co-factors for specific spatiotemporal action of RhoGEFs to activate Rho GTPases. Ack1p complexes with the RhoGEF, Rom2p, and Rho1p to activate Pkc1p. Rgl1p complexes with another RhoGEF, Tus1p, to paradoxically inhibit Pkc1p activation (Krause et al., 2012). The identification of these proteins offers another level of complexity to Rho GTPase function. Considering our evidence that Tef1p is not a downstream effector and previous results which show that it interacts with Bni1p, a known Rho1p

effector protein (Umikawa et al., 1998), and that Rho activation appears to be concurrent with calcium flux in membrane fusion (Logan et al., 2010; Eitzen et al. 2000), we propose that Tef1p may be acting as a co-factor for the spatiotemporal activation of Rho1p in membrane fusion. We propose that Tef1p may act as a calcium sensor where calcium flux induces complex formation of Tef1p with Bni1p, Rho1p and a RhoGEF, leading to activation of Bni1p activity and completion of membrane fusion (**Fig. 14**). Further evidence that Tef1p may be involved in Rho1p activation is in the case of human papilloma virus type 38 E7 protein where the E7 protein was found to inhibit the binding and bundling properties of human eEF1A (homologue of Tef1p) and lead to downstream RhoA (human homologue of Rho1p) activation (Yue et al., 2011). Additionally, we cannot ignore evidence for the role of Tef1p in Rho activation. This was shown for narciclasine, where the drug is able to bind to mammalian eEF1A and inhibit its actin bundling activity, while inducing activation of RhoA (Van Goitsenoven et al., 2010; Lefranc et al., 2009). While Van Goitsenoven et al., (2010) were able to show that narciclasine is able to directly bind to eEF1A, direct binding of narciclasine to RhoA has yet to be shown. Thus we hypothesize that the effect on RhoA activation by narciclasine may be due to actions through eEF1A. Considering the characterization of the binding of Tef1p to Bni1p defined by Umikawa et al. (1998), this suggests that Tef1p may be playing an adapter role since they found that Bni1p inhibited Tef1p actin bundling activity. They also found that the Tef1p binding region of Bni1p was

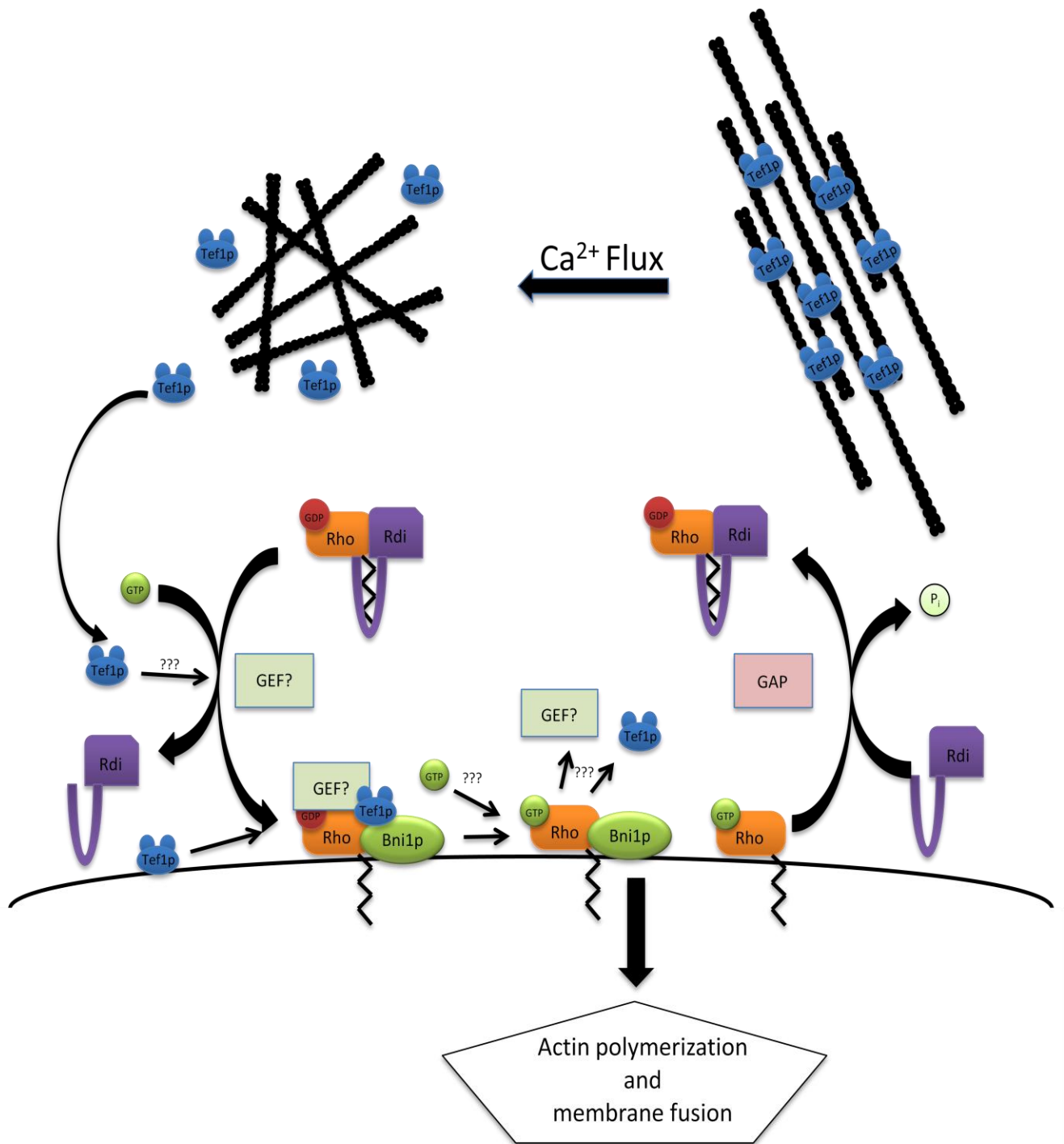


Figure 14. Model of Tef1p-Rho1p function in vacuole fusion. See *DISCUSSION* for a description of the model.

necessary for Bni1p function. They concluded that interplay of Tef1p-Bni1p association modulates the actin binding properties likely through steric inhibition, and this facilitated Rho1p stimulated actin reorganization (Umikawa et al., 1998).

With this evidence in mind we present a potential model through which Tef1p may be interacting with Rho1p during membrane fusion (**Fig. 14**). The late stages of fusion trigger a calcium flux which induces dissociation of Tef1p from actin, which would allow for interactions with downstream partners (e.g. Bni1p, Rho1p, and/or potential RhoGEFs). Whether this complex is part of a potential Rdi1p dissociation complex or the complex is formed after Rho1p is delivered to the membrane would be something worth investigating. After nucleotide exchange has occurred, we propose that Tef1p may dissociate from an active Rho1p complex, which would lead to a downstream actin polymerization step or some unknown function leading to membrane fusion.

CHAPTER 5

FUTURE DIRECTIONS

After determining that Tef1p is not a downstream effector of Rho1p, we suggest that Tef1p is involved in regulating the spatiotemporal activation of Rho1p. Dissection of a potential complex might be difficult, as it appears that several factors may be involved; however, we should first look for the presence of a RhoGEF such as Rom2p or Tus1p and Bni1p in complex with Rho1p and Tef1p. Umikawa et al., (1998) had begun to characterize the interaction between Bni1p and Tef1p. They had found that Bni1p inhibited the actin bundling properties of Tef1p; however, they were making the assumption that Bni1p was upstream of Tef1p in actin cytoskeleton reorganization. An interesting experiment would be to determine the Bni1p interacting domain of Tef1p and attempt to create a mutant that is able to bind to Rho1p but not Bni1p and to observe for cytoskeletal defects potentially due to loss of Bni1p activity. A collection of mutants of Rho1p and Tef1p will likely be needed to determine the nature of this interaction; however, we must first identify the regions of Rho1p and Tef1p that are interacting, which we have found to be a difficult task. Performing a co-immunoprecipitation against GFP using the GFP-Tef1p domain constructs and looking for endogenous Rho1p interaction may provide better insight into the domain interaction. There is also more additional investigation needing to be performed into the potential role of calcium/calmodulin in Rho1p activation. Preliminary experiments performed in the Eitzen lab (not shown) suggest that calcium/calmodulin is able to enhance the activation of Rho1p. Future work needs to be performed to investigate if the effect of

calcium/calmodulin is occurring through Tef1p. Currently, there is no evidence to suggest that calcium/calmodulin binds directly to Rho1p, but this is something that we should investigate. If we find that calcium/calmodulin does not directly bind to Rho1p, we would suggest that Tef1p is potentially acting as a calcium/calmodulin sensor/adaptor.

CHAPTER 6

CONCLUSIONS

In conclusion, we have found that Tef1p does not appear to be a downstream effector of Rho1p, but may be involved in upstream signaling leading to specific spatiotemporal activation of Rho1p. Identification of additional binding partners such as a RhoGEF in a functional complex with Tef1p and Rho1p would offer support for our future hypothesis that Tef1p acts to functionally specify the role of Rho1p spatiotemporally in membrane fusion.

CHAPTER 7

REFERENCES

- Aghazadeh, B., Zhu, K., Kubiseski, T. J., Liu, G. A., Pawson, T., Zheng, Y., & Rosen, M. K. (1998). Structure and mutagenesis of the Dbl homology domain. *Nat Struct Biol*, 5(12), 1098–107.
- Andersen, G. R., Nissen, P., & Nyborg, J. (2003). Elongation factors in protein biosynthesis. *Trends Biochem Sci*, 28(8), 434–41.
- Benard, V. (1999). Characterization of Rac and Cdc42 Activation in Chemoattractant-stimulated Human Neutrophils Using a Novel Assay for Active GTPases. *J Biol Chem*, 274, 13198–204.
- Bishop, A. L. & Hall, A. (2000). Rho GTPases and their effector proteins. *The Biochem J*, 348, 241–55.
- Bradford, M. M. (1976). A Rapid and Sensitive Method for the Quantitation of Microgram Quantities of Protein Utilizing the Principle of Protein-Dye Binding. *Anal Biochem*, 72, 248–54.
- Brieher, W. (2013). Mechanisms of actin disassembly. *Mol Biol Cell*, 24(15), 2299–302.
- Eitzen, G, Thorngren, N., & Wickner, W. (2001). Rho1p and Cdc42p act after Ypt7p to regulate vacuole docking. *EMBO J*, 20(20), 5650–6.
- Eitzen, G, Will, E., Gallwitz, D., Haas, a, & Wickner, W. (2000). Sequential action of two GTPases to promote vacuole docking and fusion. *EMBO J*, 19(24), 6713–20.
- Eitzen, G. (2003). Actin remodeling to facilitate membrane fusion. *BBA-Mol Cell Res*, 1641, 175–81.
- Eitzen, G, Wang, L., Thorngren, N., & Wickner, W. (2002). Remodeling of organelle-bound actin is required for yeast vacuole fusion. *J Cell Biol*, 158(4), 669–79.
- Elsaraj, S. M., & Bhullar, R. P. (2008). Regulation of platelet Rac1 and Cdc42 activation through interaction with calmodulin. *Biochim Biophys Acta*, 1783, 770–8.
- Gamblin, S. J., & Smerdon, S. J. (1998). GTPase-activating proteins and their complexes. *Curr Opin Struc Biol*, 8, 195–201.
- Gross, S. R., & Kinzy, T. G. (2007). Improper organization of the actin cytoskeleton affects protein synthesis at initiation. *Mol Cell Biol*, 27(5), 1974–89.

- Haas, A., Schegimann, D., Lazar, T., Gallwitz, D., & Wickner, W. (1995). The GTPase Ypt7p. *EMBO J*, *14*(21), 5258–70.
- Hayashi, H., & Edobashi, S. (1980). Calcium-Regulated Smooth Muscle Modulator Protein Interacting Agents Inhibit Protein Kinase and ATPase. *Mol Pharm*, *17*, 66–72.
- Isgandarova, S., Jones, L., Forsberg, D., Loncar, A., Dawson, J., Tedrick, K., & Eitzen, G. (2007). Stimulation of actin polymerization by vacuoles via Cdc42p-dependent signaling. *J Biol Chem*, *282*(42), 30466–75.
- Jaffe, A. B., & Hall, A. (2005). Rho GTPases: biochemistry and biology. *Annu Rev Cell Dev Bi*, *21*, 247–69.
- Jansen, G., Wu, C., Schade, B., Thomas, D. Y., & Whiteway, M. (2005). Drag&Drop cloning in yeast. *Gene*, *344*, 43–51.
- Jones, L., Tedrick, K., Baier, A., Logan, M. R., & Eitzen, G. (2010). Cdc42p is activated during vacuole membrane fusion in a sterol-dependent subreaction of priming. *J Biol Chem*, *285*(7), 4298–306.
- Krause, S., Cundell, M., & Poon, P. (2012). Functional specialisation of yeast Rho1 GTP exchange factors. *J Cell Sci*, *125*, 2721–31.
- Lefranc, F., Sauvage, S., Van Goietsenoven, G., Mégalizzi, V., Lamoral-Theys, D., Debeir, O., ... Kiss, R. (2009). Narciclasine, a plant growth modulator, activates Rho and stress fibers in glioblastoma cells. *Mol Cancer Ther*, *8*(7), 1739–50.
- Logan, M. R., Jones, L., & Eitzen, G. (2010). Cdc42p and Rho1p are sequentially activated and mechanistically linked to vacuole membrane fusion. *Biochem Biophys Res C*, *394*, 64–9.
- Maitra, S., & Nowick, J. (2000). β -Sheet interactions between proteins. *The Amide Linkage: Structural Significance in Chemistry, Biochemistry, and Materials Science*, 495–518.
- Malacombe, M., Bader, M.-F., & Gasman, S. (2006). Exocytosis in neuroendocrine cells: new tasks for actin. *Biochim Biophys Acta*, *1763*, 1175–83.
- Morita, K., Bunai, F., & Numata, O. (2008). Roles of three domains of Tetrahymena eEF1A in bundling F-actin. *Zool Sci*, *25*(1), 22–9.

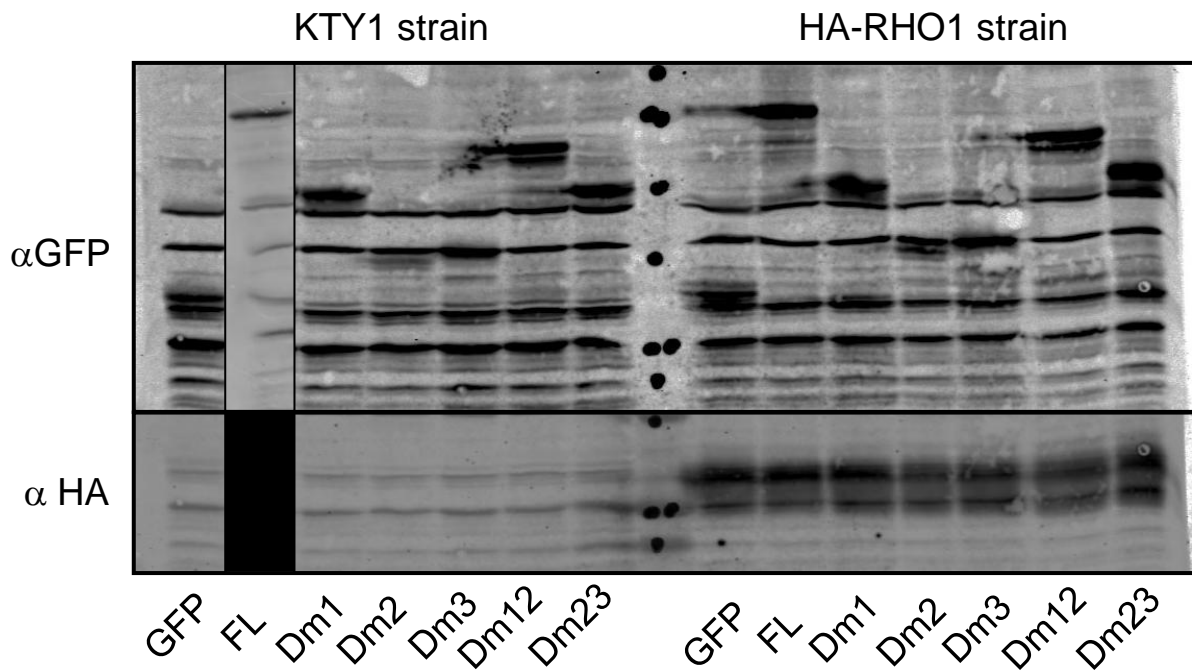
- Moseley, J. B., & Goode, B. L. (2006). The yeast actin cytoskeleton: from cellular function to biochemical mechanism. *Microbiol Mol Biol R*, *70*(3), 605–45.
- Munshi, R., Kandl, K. a, Carr-Schmid, A., Whitacre, J. L., Adams, A.E., & Kinzy, T. G. (2001). Overexpression of translation elongation factor 1A affects the organization and function of the actin cytoskeleton in yeast. *Genetics*, *157*, 1425–36.
- Osawa, M., Swindells, M. B., Tanikawa, J., Tanaka, T., Mase, T., Furuya, T., & Ikura, M. (1998). Solution structure of calmodulin-W-7 complex: the basis of diversity in molecular recognition. *J Mol Biol*, *276*, 165–76.
- Owen, C., Derosier, D., & Condeelis, J. (1992). Actin crosslinking protein EF-1a of *Dictyostelium discoideum* has a unique bonding rule that allows square-packed bundles. *J Struc Biol*, *109*, 248–54.
- Peters, C., & Mayer, A. (1998). Ca²⁺/calmodulin signals the completion of docking and triggers a late step of vacuole fusion. *Nature*, *396*, 575–80.
- Pittman, Y. R., Kandl, K., Lewis, M., Valente, L., & Kinzy, T. G. (2009). Coordination of eukaryotic translation elongation factor 1A (eEF1A) function in actin organization and translation elongation by the guanine nucleotide exchange factor eEF1B α . *J Biol Chem*, *284*(7), 4739–47.
- Price, A, Seals, D., Wickner, W., & Ungermann, C. (2000). The docking stage of yeast vacuole fusion requires the transfer of proteins from a cis-SNARE complex to a Rab/Ypt protein. *J Cell Biol*, *148*(6), 1231–8.
- Ren, X., Kiosses, W. B., & Schwartz, M. A. (1999). Regulation of the small GTP-binding protein Rho by cell adhesion and the cytoskeleton. *EMBO J*, *18*(3), 578–85.
- Rossman, K. L., & Sondek, J. (2005). Larger than Dbl: new structural insights into RhoA activation. *Trends Biochem Sci*, *30*(4), 163–5.
- Sahai, E., Alberts, A. S., & Treisman, R. (1998). RhoA effector mutants reveal distinct effector pathways for cytoskeletal reorganization, SRF activation and transformation. *EMBO J*, *17*(5), 1350–61.
- Soares, D. C., Barlow, P. N., Newbery, H. J., Porteous, D. J., & Abbott C. M. (2009). Structural models of human eEF1A1 and eEF1A2 reveal two distinct surface clusters of sequence variation and potential differences in phosphorylation. *PLOS one*, *4*(7), e6315.

- Spector, I., Shocket, N.R., Kashman, Y., & Groweiss, A. (1983). Latrunculins: novel marine toxins that disrupt microfilament organization in cultured cells. *Science*, *219*(4584), 492-5.
- Umikawa, M., Tanaka, K., Kamei, T., Shimizu, K., Imamura, H., Sasaki, T., & Takai, Y. (1998). Interaction of Rho1p target Bni1p with F-actin-binding elongation factor 1alpha: implication in Rho1p-regulated reorganization of the actin cytoskeleton in *Saccharomyces cerevisiae*. *Oncogene*, *16*(15), 2011-6.
- Ungermann, C., Sato, K., & Wickner, W. (1998). Determining the functions of trans -SNARE pairs. *Nature*, *396*, 543-8.
- Van Goietsenoven, G., Hutton, J., Becker, J. P., Lallemand, B., Robert, F., Lefranc, F., Pirker, C., Vandenbussche, G., Van Antwerpen, P., Evidente, A., Berger, W., Prevost, M., Pelletier, J., Kiss, R., Kinzy, T., Korneinko, A., & Mathieu, V. (2010). Targeting of eEF1A with Amaryllidaceae isocarbostryls as a strategy to combat melanomas. *FASEB J*, *24*(11), 4575-84.
- Van Goietsenoven, G., Mathieu, V., Lefranc, F., Kornienko, A., Evidente, A., & Kiss, R. (2013). Narciclasine as well as other Amaryllidaceae isocarbostryls are promising GTPase targeting agents against brain cancers. *Med Res Rev*, *33*(2), 439-55.
- Wickner, W., & Haas, A. (2000). Yeast homotypic vacuole fusion: a window on organelle trafficking mechanisms. *Annu Rev Biochem*, *69*, 247-75.
- Xu, Z., Sato, K., & Wickner, W. (1998). LMA1 binds to vacuoles at Sec18p (NSF), transfers upon ATP hydrolysis to a t-SNARE (Vam3p) complex, and is released during fusion. *Cell*, *93*, 1125-34.
- Yang, F., Demma, M., Warren, V., Dharmawardhane, S., & Condeelis, J. (1990). Identification of an actin-binding protein from *Dictostelium* as elongation factor 1a. *Nature*, *347*, 494-6.
- Yue, J., Shukla, R., Accardi, R., Zanella-Cleon, I., Siouda, M., Cros, M.-P., ... Sylla, B. S. (2011). Cutaneous human papillomavirus type 38 E7 regulates actin cytoskeleton structure for increasing cell proliferation through CK2 and the eukaryotic elongation factor 1A. *J Virol*, *85*(17), 8477-94.
- Zhang, B., Zhang, Y., Wang, Z., & Zheng, Y. (2000). The role of Mg²⁺ cofactor in the guanine nucleotide exchange and GTP hydrolysis reactions of Rho family GTP-binding proteins. *J Biol Chem*, *275*(33), 25299-307.

Zigmond, S. H. (2004). Formin-induced nucleation of actin filaments. *Current opinion in Cell Biology*, 16, 99–105.

Appendix A

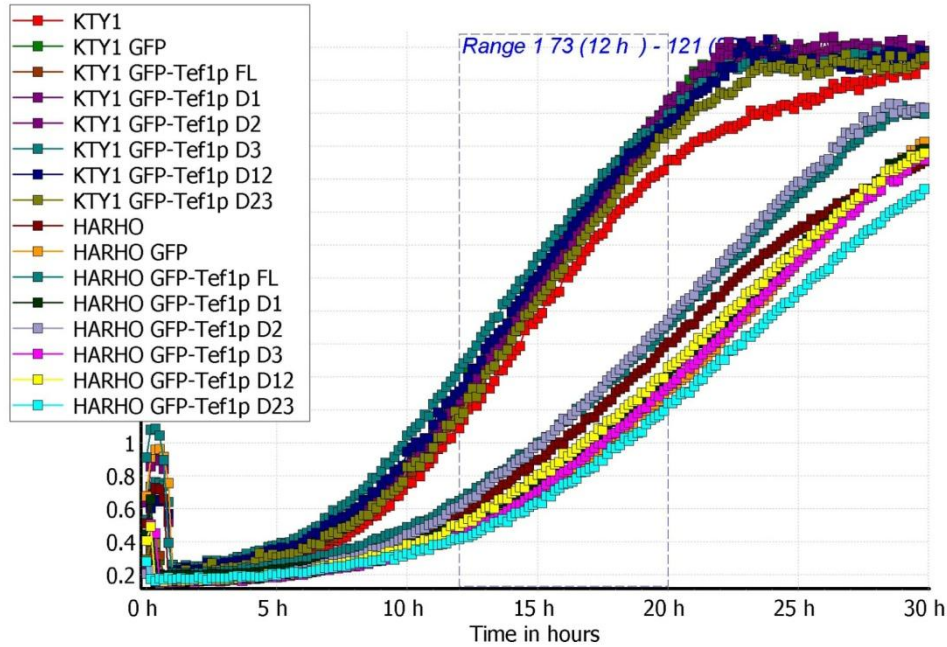
Growth Curve Data



Confirmation of GFP-Tef1p full-length and sub-domain expression in the KTY1 and HA-RHO1 strains.. Confirmation of expression was by whole cell lysis of 0.25 OD units per stain. Extracted proteins were analyzed by SDS-PAGE and immunoblot analysis using GFP and HA antibodies.

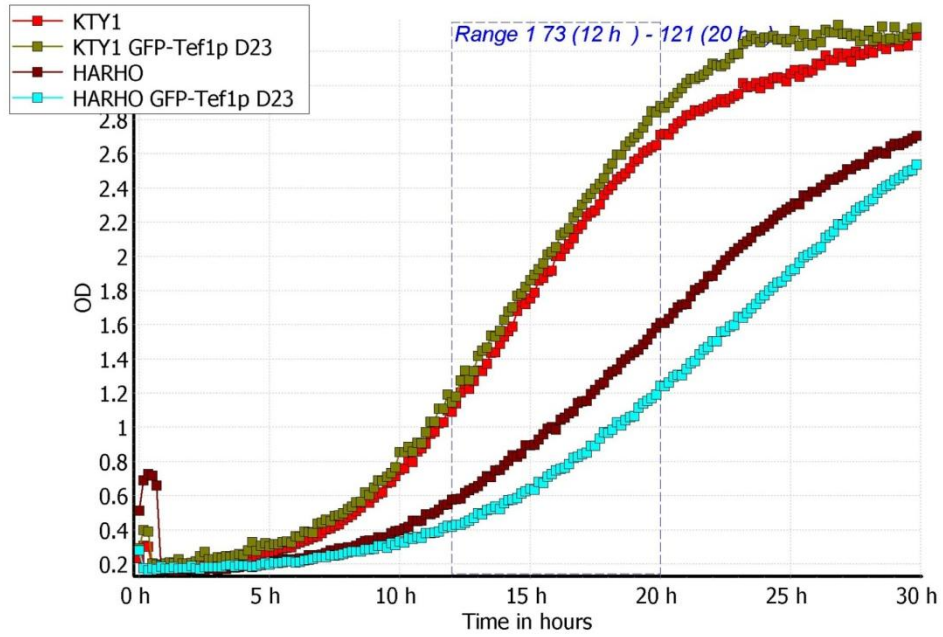
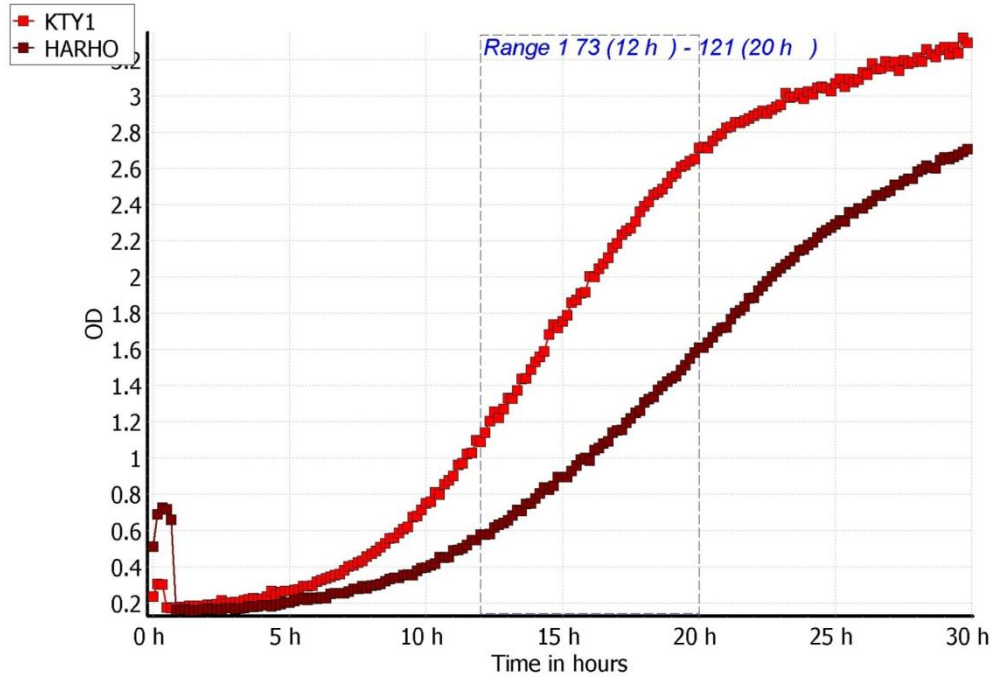
Appendix B

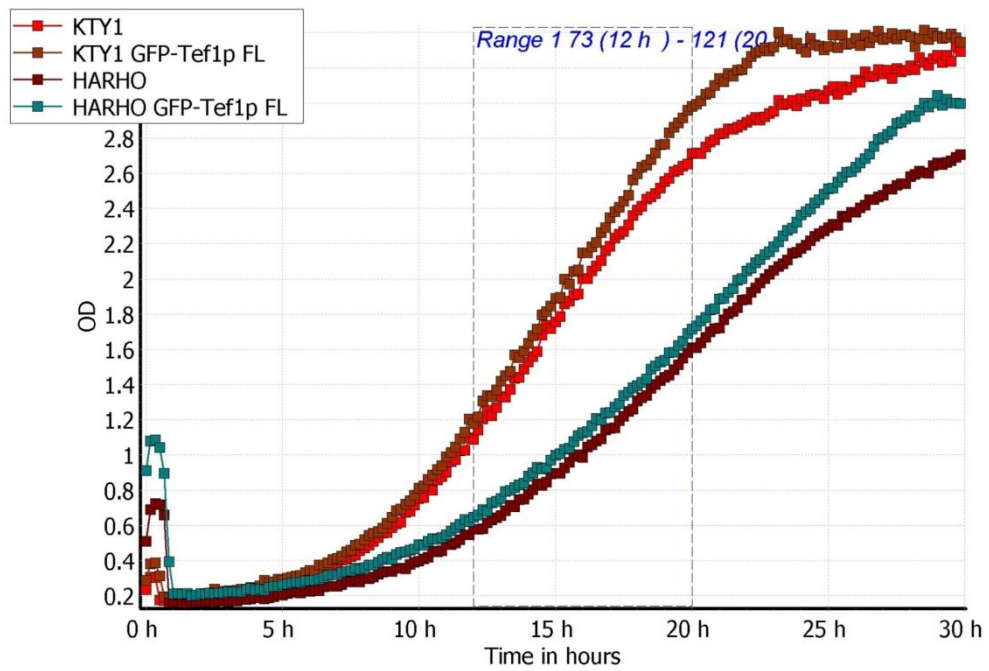
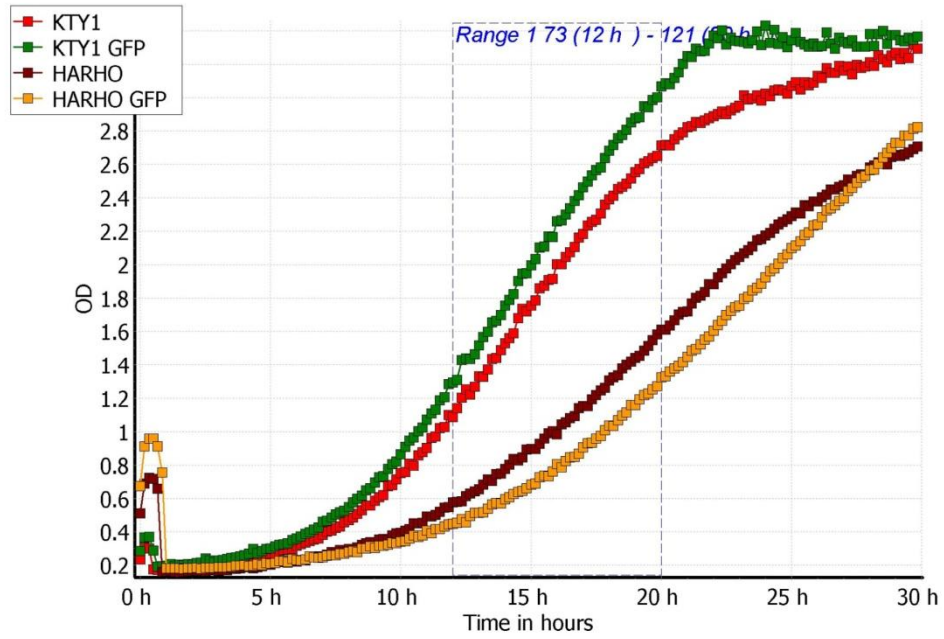
Growth Curve Data

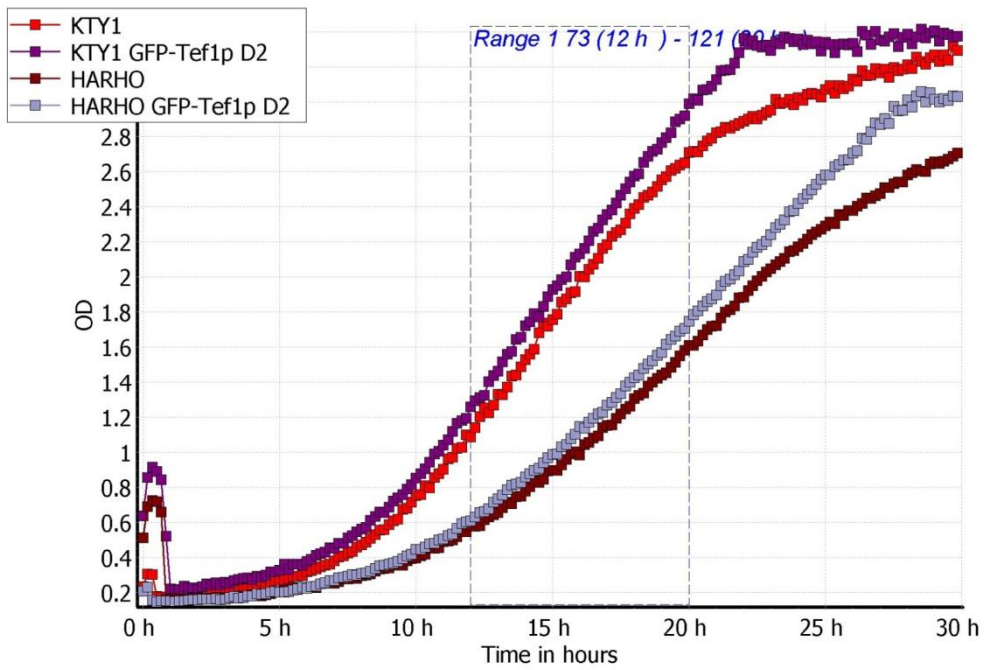
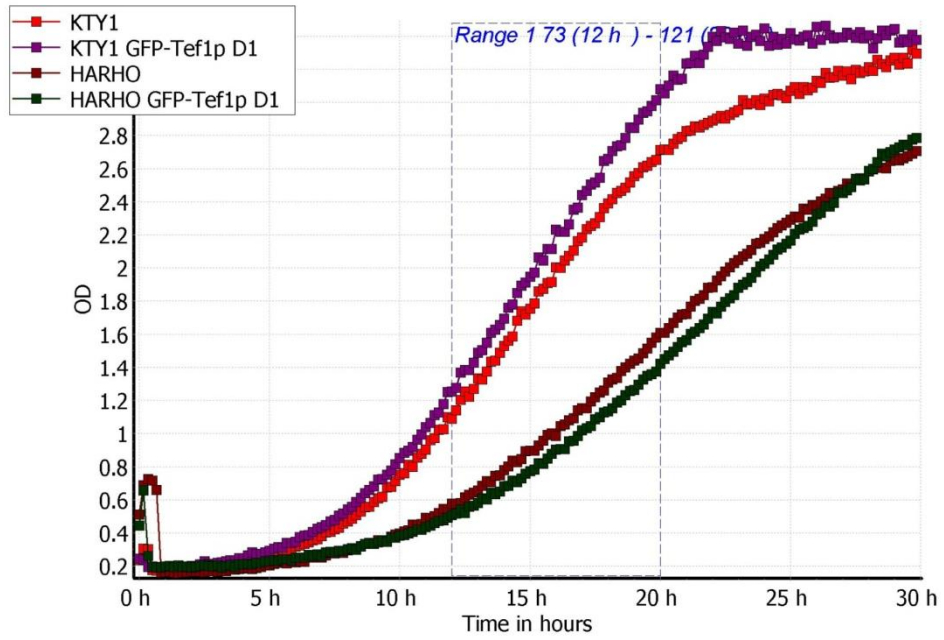


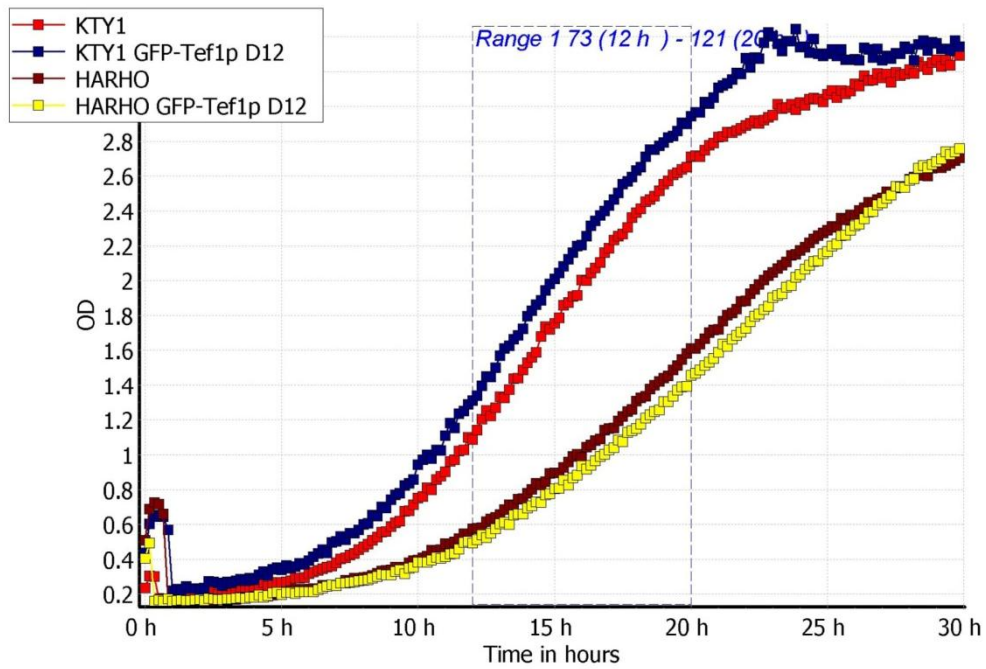
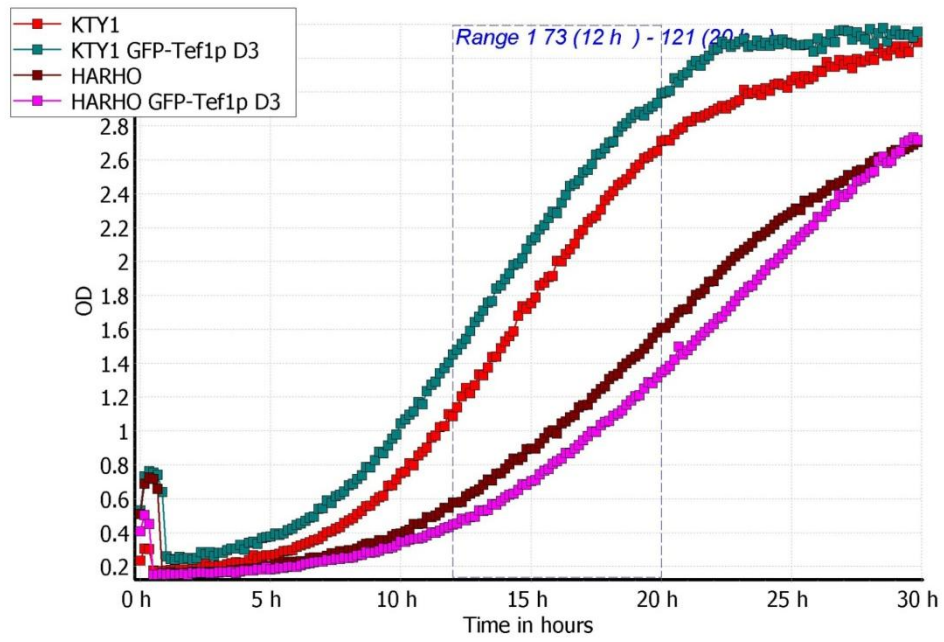
Construct	Doubling Time, DT (h)		Δ DT (construct vs none)	
	KTY1	HA-RHO1	KTY1	HA-RHO1
none	2.89	4.51		
GFP	2.77	4.78	-0.12	0.27
GFP-Tef1p FL	2.81	4.38	-0.08	-0.13
GFP-Tef1p Dm1	2.72	5.01	-0.17	0.50
GFP-Tef1p Dm2	2.86	4.26	-0.03	-0.25
GFP-Tef1p Dm3	2.99	4.90	0.10	0.39
GFP-Tef1p Dm12	2.96	4.93	0.07	0.42
GFP-Tef1p Dm23	2.80	5.28	-0.09	0.77

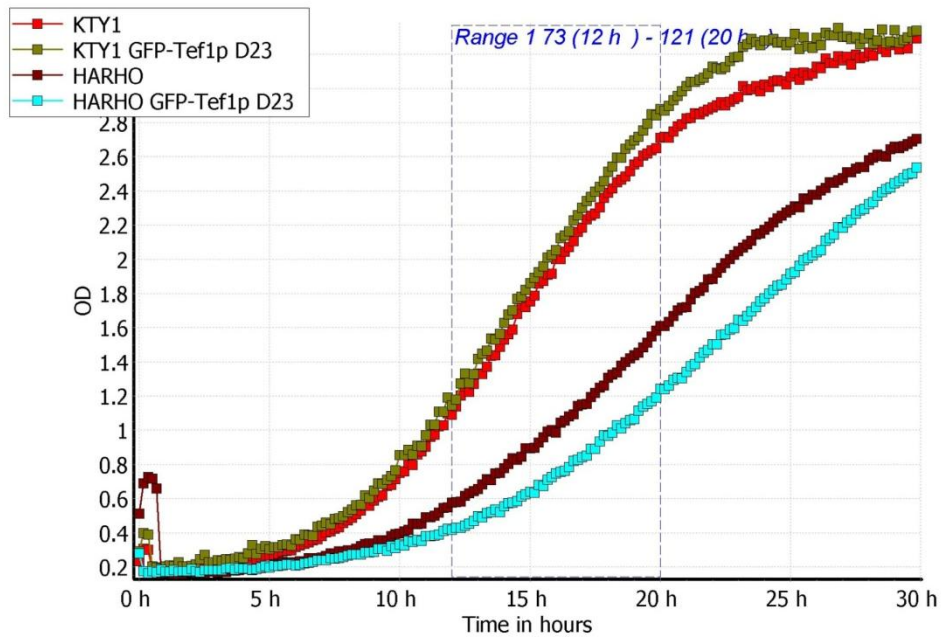
Effect of GFP-Tef1p full-length and sub-domain expression on growth rates of wild-type and HA-RHO1 overexpressing yeast. Wild-type yeast (KTY1) and yeast over-expressing 3xHA-Rho1p (HA-RHO1) were examined for changes in growth rates when transformed with constructs expressing GFP-Tef1p full-length and sub-domains as indicated in Figure 5A. Strains were incubated at 30°C in a CLARIOstar plate reader with agitation and optical density was measured at 600 nm over 30 h at 10 min intervals. Doubling time was determined by taking the maximum slope over a 12 time point range between 12 h and 20 h.











Construct	Doubling Time, DT (h)		Δ DT (construct vs none)	
	KTY1	HA-RHO1	KTY1	HA-RHO1
none	2.89	4.51		
GFP	2.77	4.78	-0.12	0.27
GFP-Tef1p FL	2.81	4.38	-0.08	-0.13
GFP-Tef1p Dm1	2.72	5.01	-0.17	0.50
GFP-Tef1p Dm2	2.86	4.26	-0.03	-0.25
GFP-Tef1p Dm3	2.99	4.90	0.10	0.39
GFP-Tef1p Dm12	2.96	4.93	0.07	0.42
GFP-Tef1p Dm23	2.80	5.28	-0.09	0.77